

Governors State University

OPUS Open Portal to University Scholarship

All Student Theses

Student Theses

Fall 2023

Autodocking Studies of Oxygenated Fullerenes as Inhibitors of The HIV Protease

Michael Kaminski

Follow this and additional works at: <https://opus.govst.edu/theses>



Part of the [Chemistry Commons](#), and the [Medical Biochemistry Commons](#)

For more information about the academic degree, extended learning, and certificate programs of Governors State University, go to http://www.govst.edu/Academics/Degree_Programs_and_Certifications/

Visit the [Governors State Analytical Chemistry Department](#)

This Thesis is brought to you for free and open access by the Student Theses at OPUS Open Portal to University Scholarship. It has been accepted for inclusion in All Student Theses by an authorized administrator of OPUS Open Portal to University Scholarship. For more information, please contact opus@govst.edu.

Autodocking Studies of Oxygenated Fullerenes as Inhibitors of The HIV Protease

By

Michael Kaminski

B.S., Saint Xavier University, 2021

THESIS

Submitted in partial fulfillment of the requirements

For the Degree of Master of Science,
With a Major in Analytical Chemistry

2023

ACKNOWLEDGEMENTS

Dr. Shelly Kumar, my professor and mentor who has guided me throughout my research.

My professors at both Governors State University and Saint Xavier University for teaching me the skills to become the scientist I am today.

My parents Vicki and Allan Kaminski for encouraging me and helping push me forward in my academic career.

TABLE OF CONTENTS

Abstract.....	1
Introduction.....	3
AutoDock Software.....	4
Research on HIV-Protease Inhibition via Molecular Docking.....	5
History of HIV-Protease Inhibition Using Functionalized Fullerenes.....	6
Goals and Objectives.....	7
Methods.....	9
Software Used.....	9
Hardware.....	9
Installing The Software.....	9
Acquiring pdb Files.....	9
Preparation For Docking.....	10
Output and Log Files.....	14
Making Oxygenated C ₆₀ In Spartan.....	15
Electrostatic Potential Map in Spartan.....	18
HIV-Protease Analysis with PyMOL.....	20
Results.....	23
Discussion	47
Conclusion.....	50
References.....	51

LIST OF TABLES

Table 1. The C ₆₀ O _x Structures Studied and Documented	22
Table 2. C ₆₀ O Docking Results.....	23
Table 3. C ₆₀ O ₂ Docking Results.....	26
Table 4. C ₆₀ O ₄ -G Docking Results.....	29
Table 5. C ₆₀ O ₄ -E Docking Results.....	32
Table 6. C ₆₀ O ₆ -G Docking Results	35
Table 7. C ₆₀ O ₆ -E Docking Results	38
Table 8. C ₆₀ O ₈ -G Docking Results	41
Table 9. C ₆₀ O ₈ - Docking Results	44

LIST OF FIGURES

Figure 1. Ozonolysis of C ₆₀ in the presence of <i>p</i> -xylene.....	7
Figure 2. 5CON HIV-PR in AutoDock Tools.....	11
Figure 3. Grid box with adjustable location/size in AutoDock Tools.....	11
Figure 4. Configuration File for Docking.....	13
Figure 5. Command Prompt of Executed Docking For Trial Run	13
Figure 6. Docking Log file Output Example.....	14
Figure 7. Making of Buckminsterfullerene (C ₆₀) in Spartan.....	15
Figure 8. Electrostatic potential map for C ₆₀ O ₂ with modified energy boundaries	19
Figure 9. C ₆₀ O ₄ -E created by placing carbonyls at electrophilic sites	19
Figure 10. HIV-PR ribbon form in PyMOL.....	20
Figure 11. PyMOL analysis of H-bonds between C ₆₀ O ₄ and HIV-PR residues	21
Figure 12. C ₆₀ O Blind Docking Conformations and Interactions.....	24
Figure 13. C ₆₀ O ₂ Blind Docking Conformations and Interactions.....	27
Figure 14. C ₆₀ O ₄ -G Blind Docking Conformations and Interactions.....	30
Figure 15. C ₆₀ O ₄ -E Blind Docking Conformations and Interactions.....	33
Figure 16. C ₆₀ O ₆ -G Blind Docking Conformations and Interactions.....	36
Figure 17. C ₆₀ O ₆ -E Blind Docking Conformations and Interactions.....	39
Figure 18. C ₆₀ O ₈ -G Blind Docking Conformations and Interactions.....	42
Figure 19. C ₆₀ O ₈ -E Blind Docking Conformations and Interactions.....	45
Figure 20. Hydrogen Bonded Residues in Docking Studies.....	48
Figure 21. HIV-PR in PyMOL Comparing Active and Common Binding Sites.....	49

KEY WORDS

AIDS: Acquired Immunodeficiency Syndrome, a deadly chronic disease that occurs from untreated HIV. The immune system becomes damaged and is unable to defend against diseases.

Amino Acid Residue: The term for individual amino acids that have lost water in the process of linking together during protein formation.

AutoDock: A docking software developed by Oleg Trott and Arthur J. Olson at The Scripps Research Institute for simulating interactions between macromolecules and ligands.

Blind Docking: The act of performing a simulated molecular docking experiment without specifying where the ligand is supposed to bind to the macromolecule.

Buckminsterfullerene: A compound made up of sixty carbon atoms with a soccer ball-like appearance.

Cytotoxicity: A measure of how much damage a compound will cause to cells in the body.

Docking: The simulation of how a ligand binds to a macromolecule or substrate. Docking programs are a form of molecular modeling commonly used for drug discovery and research.

HIV: Human Immunodeficiency Virus, a sexually transmitted virus (also transmitted via blood contact with an infected person) that will cause AIDS if unable to be treated. No cure exists, so treatments focus on reducing the number of viruses in the blood (referred to as “viral load”).

Oxygenation: A reaction pathway that adds oxygen(s) to a compound(s).

Protease (PR): An enzyme that catalyzes the breakdown of larger proteins and is instrumental to the development of a mature virus or cell.

Pdb File: A Protein Database file format that contains the structure of a compound examined via X-Ray Crystallography

PyMOL: A molecular modeling software used for analyzing docking output files and hydrogen bonds.

Abstract

In a previous study, several oxygenated fullerene compounds were produced by ozonation of C₆₀ (Buckminsterfullerene) and were identified by elemental analysis and by SALI (surface analysis by laser ionization). Some of these compounds, especially a batch, SK-5, a mixture of C₆₀O₁₋₈, were shown to inhibit activities of HIV-Protease with IC₅₀ (concentration for 50% inhibition) of 1 mg/mol in the in-vitro studies. The oxygenated fullerenes were shown to have epoxide, ketones, and hydroxyl functionalities. As expected, C₆₀ interacted with ozone with alkene functionality and not as an aromatic compound. It was postulated that C₆₀O had epoxide functionality, as a product of ozonation of one of the double bonds of C₆₀; C₆₀O₂ had ketone functionalities by Ozonolysis of one of the double bonds of C₆₀; C₆₀O₄, C₆₀O₆, C₆₀O₈ had ketone functionalities by Ozonolysis of successive double bonds of C₆₀. The hydroxyl functionality was likely produced due to interaction of water and the oxygenated fullerenes. In the present study, the interactions of oxygenated fullerenes (small molecules) with HIV-Protease (macromolecules) at the molecular levels were studied via blind docking using AutoDock Vina software to elucidate the mechanism of these interactions. The structures of C₆₀O, C₆₀O₂, C₆₀O₄, C₆₀O₆, C₆₀O₈ were generated using Spartan software and were docked with a crystal structure of the HIV-Protease (PR) obtained from The Brookhaven Protein Data Bank using AutoDock Vina. These docking studies showed that the oxygenated fullerenes bound to multiple sites of the HIV-PR with high binding affinities (-10.4 to -8.1 kcal/mol). Nine docking poses were generated for each structure, and the models of each conformation were studied using PyMOL software. The docking models in PyMOL suggest that the high binding affinity is a result of the abundance of strong hydrogen bonds ~2.3Å long across the various C₆₀O_x structures. The presence of dipole-dipole and van der waals interactions were also found to have played a significant role in binding, with several conformations exhibiting strong binding (≥ -9.8 kcal/mol) with no hydrogen bonds. Results indicate a strong correlation between the ability of C₆₀O_x to produce hydrogen bonds/strong dipole interaction with the HIV-PR and inhibition efficacy.

Introduction

In 2004, the global mortality rate from the HIV/AIDS epidemic reached an all-time high of 1.84 million deaths worldwide. As various pharmaceutical drug treatments have improved and become more available with time, the mortality rate has become less than half of what it was. In 15 years, the global mortality rate dropped to 863,838 deaths in 2019.¹ Despite the fact that these statistics do display an improvement in the understanding of HIV and possible treatments, the research dedicated towards ending the AIDS epidemic is far from over. Because there is no cure for HIV, current treatments focus on reducing the amount of the HIV virus present in the blood (viral load) through a process called antiretroviral therapy.² Treatments can accomplish this task through several different mechanisms: Nucleoside reverse transcriptase inhibitors (NRTI), non-nucleoside reverse transcriptase inhibitors (NNRTI), protease inhibitors, integrase inhibitors, fusion inhibitors, post-attachment inhibitors, and pharmacokinetic enhancers.^{3,4} Treatments will consist of multiple medications that encompass many of these pathways to reducing the HIV viral load. Several compounds boasting low cytotoxicity ($< 100\mu\text{M}$ CC_{50} , concentration for 50% cell toxicity) that impede HIV replication have been validated as effective drug treatments. Unfortunately, repeated use of these medications has resulted in a sharp increase of drug-resistant strains of the HIV virus. In 2018, the World Health Organization (WHO) reported that 3 in 10 adults and 5 in 10 children beginning antiretroviral therapy possess drug-resistant viruses.⁵ As time goes on, the current medication becomes increasingly less effective even for people who had previously benefited from these treatments. Furthermore, several courses of medication lead to various complications such as an increase in chronic renal diseases and bone density loss.⁴ Consequently, the research and development of new antiretroviral compounds becomes more significant each day for treating these drug-resistant viruses.

In this study, the work done by Kumar on a HIV-protease inhibitor composed of multiple oxygenated Buckminsterfullerene compounds is expanded upon using docking software AutoDock Vina.^{6,7} These oxygenated fullerene compounds were synthesized via ozonolysis of the alkenes present in C_{60} in the presence of *p*-xylene. By examining the interactions of oxygenated C_{60} (C_{60}O_x) with the HIV-PR in AutoDock, a better understanding of the inhibition process can be obtained.

AutoDock Software

AutoDock encompasses a variety of programs that serve as automated virtual tools for docking. AutoDock simulates the non-covalent binding of various substrates, drugs etc. to 3D macromolecules.⁸ Both the macromolecule (receptor) and the small molecule (ligand) used are pdb (Protein Database) files. Structures of macromolecules from x-ray crystallography are converted to pdb files and can be downloaded from websites such as RCSB.org (The Brookhaven Protein Data Bank).⁹ Smaller ligand structures can be created in 3D modeling programs like Spartan and converted to pdb format for use in AutoDock. In AutoDock, the pdb files must be converted to pdbqt (“Q” for partial charge, and T for atom type) format using AutoDock Tools (a graphical interface program for AutoDock). There are two versions of AutoDock available: AutoDock 4 and AutoDock Vina. Both versions make use of AutoDock Tools. The primary difference between AutoDock 4 and AutoDock Vina is that the former is composed of two applications: AutoDock performs the docking in accordance with the user made grid maps in AutoDock Tools; Autogrid pre-calculates the projected grids. AutoDock Vina simplifies the docking process by calculating the grid maps internally thereby circumventing the need for Autogrid entirely. AutoDock Vina makes use of multithreading which allows it to take advantage of multiple core processing unit (CPU) cores to augment the speed of the docking. On an 8-core CPU, benchmark tests for AutoDock Vina ran nearly 450 times faster than AutoDock 4.¹⁰ After the docking is complete, the binding affinities based on the nine most stable ligand-receptor docking poses are output as a text (txt) file for the user. This data is generated from a scoring function that utilizes empirical information from the receptor-ligand complexes and experimental binding affinity measurements.¹⁰ Both AutoDock 4 and Vina utilize empirically weighted scoring functions that view the same parameters (hydrogen bonds, rotatable ligand bonds etc.).⁹ Both programs employ the same type of global search algorithms to gather the data used in the scoring functions, but AutoDock Vina boasts a more optimized local search methodology. This allows Vina to perform more calculations to generate more accurate binding affinities for conformations containing ligands with high numbers of rotatable bonds^{10,11}. Once the docking is complete, the scoring function additionally provides an output pdbqt file. This file can be opened in a program such as PyMOL to view and interact with all docking poses generated in the docking process. According to a study performed by Su et al. AutoDock Vina was consistently ranked as possessing the most accurate and precise scoring function when

compared to other scoring functions in a variety of tests.¹² All versions of AutoDock and affiliated software are available for free use. These features of AutoDock Vina made it the ideal program for this study.

Research on HIV-Protease Inhibition via Molecular Docking

Inhibition of the HIV-PR serves as a common target for docking studies researching HIV antiretroviral treatments. Examples of this can be seen in the study performed by Razzaghi et al. on Amprenavir's binding conformations to HIV in AutoDock 4, or in Arthur J. Olson's FightAIDS@home volunteer computing project.^{13,14}

Amprenavir is one of several well documented, effective treatments for HIV.¹⁵ Although Amprenavir's efficacy and mechanism is well known, Razzaghi et al.'s docking simulations provide a methodology in which to view the binding interactions more closely¹³. Amprenavir was used as the control variable to examine the effect flexibility of the HIV-1 protease (HIV-1 PR) has on docking and inhibition. Ensemble docking was performed using AutoDock 4 with a myriad of different HIV-1 crystallographic structures obtained from the Brookhaven Protein Data Bank. Lipophilic and hydrogen bonds were examined and quantified across the different HIV-1 PR structures and their respective conformations of the docked Amprenavir ligand.¹³

In contrast to the focused approach of Razzaghi et al.'s study on examining one facet of the HIV-PR¹³, the FightAIDS@Home project (FAAH) by Arthur J. Olson utilizes AutoDock for a broader analysis¹⁴. This project utilizes the computational prowess of thousands of volunteers' computers to screen an impressive number of ligands in docking simulations against the HIV-PR. Volunteer computing is achieved through running a program in the background on a volunteer's computer. The FAAH program is installed on over 450,000 computers. With this power, approximately 10,000 ligand structures binding affinities are tested per day across hundreds of different HIV-PR structures. From 2002 to 2007, this project validated over 1000 potential drug candidates for HIV antiretroviral therapy.¹⁴ FAAH is currently in its second phase and has expanded its studies to other aspects of HIV docking such as inhibition via binding at allosteric sites.¹⁶ Despite the vastly different approach in Razzaghi et al.'s focused study using a known inhibitor¹³, and FAAH's massive amounts of tests with unknown compounds¹⁴, both experiments demonstrate the versatility and efficacy of AutoDock's ability to study HIV-PR inhibition.

History of HIV-Protease Inhibition Using Functionalized Fullerenes

The previous works utilizing AutoDock are all from the past 20 years, but the use of functionalized fullerenes in HIV-PR inhibition studies stretches further back into the 1990s with various laboratory experiments. In 1993, Schinazi et al. discovered a synthesis route using diphenyldiazomethane to produce a water-soluble *p,p'*-bis(2-aminoethyl)diphenyl- C_{60} derivative to inhibit HIV-PR.¹⁷ Many potential HIV-PR inhibiting compounds like fullerenes suffer from poor oral bioavailability due to insolubility in water. By synthesizing a new fullerene derivative containing hydrogen bonding, the positive properties of a low toxicity HIV-PR inhibitor can be maintained whilst amending the issue of poor oral bioavailability. This work was able to produce a water soluble, low toxicity (IC_{50} 4.6 μ M) compound that demonstrated anti-HIV properties. These functionalized fullerenes were found to have properties extending beyond protease inhibition for inactivation of the HIV-PR as they also demonstrated virucidal properties. The idea behind this work was further expanded upon in research by Bosi et al. in which various bis-functionalized C_{60} isomers containing 1-8 pyrrolidine groups were synthesized to produce a water-soluble drug for HIV. Results were not as successful as the compounds exhibited unsafe levels of toxicity in human cells at concentrations of 4-15 μ M, and some isomers demonstrated inactivity against HIV-2 viruses.¹⁸

Kumar's 1994 experiments on the oxygenation of C_{60} via ozonolysis serve as another example of research using fullerenes as inhibitors.^{6,7} His work describes a route for synthesizing oxygenated fullerenes via ozonolysis. The $C_{60}O_x$ products created via ozonolysis were further explored and characterized via Surface Analysis by Laser Ionization (SALI). The ozonolysis reaction was performed in the presence of *p*-xylene to show the carbonyl oxide intermediates that formed during the reaction (as seen in Figure 1 below). These fullerene compounds displayed epoxide ($C_{60}O$) and ketone ($C_{60}O_{2-8}$) functionalities and were found to effectively inhibit the HIV-PR with IC_{50} (concentration for 50% inhibition) of 1 mg/mol during in-vitro studies. The data gathered in this study would form the basis of the present work.

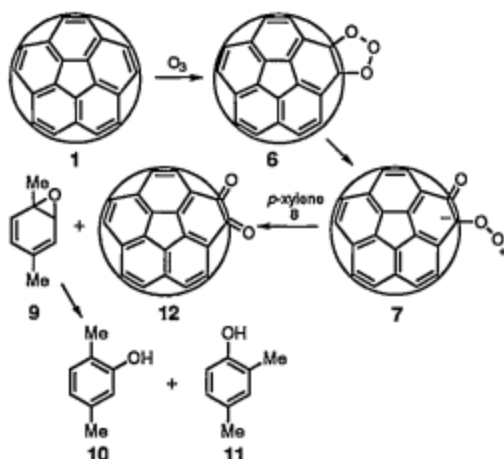


Figure 1: Ozonolysis of C_{60} in the presence of *p*-xylene

Goals and Objectives

This study continues the laboratory work of Kumar by studying the oxygenated fullerene's ability to inhibit the HIV-PR using computational modeling software.^{6,7} Razzaghi et al.'s and Olson's works demonstrate the profound ability of AutoDock to examine and validate a ligand's potential for enzyme binding and subsequent inactivation.^{10,13} In this work, AutoDock Vina was used to perform the docking of custom-built 3D models of the following compounds: $C_{60}O$, $C_{60}O_2$, $C_{60}O_4$, $C_{60}O_6$, $C_{60}O_8$. These structures were created and saved in the form of pdb files, and $C_{60}O_{4-8}$ featured two variants; One structure has the oxygens (in the form of carbonyl groups since these structures displayed ketone functionalities) positioned on opposite ends of the fullerene to create the lowest energy geometry of the structure with the lowest steric repulsion, while the other variant has the carbonyls placed at the most electrophilic sites on the structure according to the modeling software's electrostatic potential map (denoted as "G" and "E" structures respectively). This was done to accommodate for different possible bond sites of the oxygen atoms during creation of these oxygenated fullerenes in Kumar's experiments. The $C_{60}O_x$ models were built using Spartan software developed by Wavefunction Inc. Instead of focusing the grid box in AutoDock around the active site of the HIV-PR, blind docking was performed to better simulate the real laboratory experiments performed by Kumar et al. The goal of this experiment is not simply to find the binding affinity and conformation of these ligands when focused on the ideal binding location for inhibition (active site), but rather to examine if the ligand ($C_{60}O_x$) is selective to the binding site or able to bind to it at all. It is already known

that C₆₀O_x inhibits the HIV-PR; the only question left is *how* these fullerenes bind to the HIV-PR to cause inhibition. Blind docking can often be an issue to accomplish due to requiring a higher amount of computational power and time to perform, but a high-power CPU utilized by AutoDock Vina mitigates this issue.¹⁹ Blind docking produces the most stable (and therefore common) energy conformations, and this can result in the positions of the ligand being quite varied from one another with high RMSD (Root Mean Square Deviation) values (~8.14) relative to the most stable conformation. The RMSD values provide a metric of the relative distance each conformation deviates from the most stable docking pose (explained more in depth on page 14 under Methods). In addition to examining the HIV-PR itself, this experiment will also determine the efficacy of AutoDock Vina's ability to gather this data using blind docking on modern hardware under default docking configuration parameters. The same crystallographic HIV structure (5CON) obtained from Aoki et al.'s pdb file on The Brookhaven Protein Data Bank was used in all experiments. This structure was chosen because it is an unmodified wild-type protease structure. The generated output files from the docking were opened in PyMOL. This is where the conformations and hydrogen bonds of the ligands were analyzed and captured via screenshots. The experiment from Kumar et al. achieved the most inhibition from C₆₀O₁₋₈ compounds; this docking experiment should therefore display the high binding affinity to HIV-PR for those compounds. C₆₀O₃, C₆₀O₅, and C₆₀O₇ were not analyzed in this study. The goal of this study is to contribute to the base of knowledge for both HIV-PR inhibition and the abilities of AutoDock to study enzyme-ligand interactions via molecular docking. Proficiency with molecular modeling software can provide a better understanding of how these structures behave as a ligand in the presence of wild-type HIV viruses at the molecular level. This knowledge will help elucidate the properties that make for an effective antiretroviral medication.

Methods:

Software Used

AutoDock Vina is the program that executes the docking itself. It was installed in a folder alongside AutoDock MGL Tools. AutoDock Vina boasts advantages over the previous version of AutoDock (AutoDock 4) due to its ability to generate the map files during the docking process, utilize multiple CPU cores, and streamline the docking process.

AutoDock MGL Tools is the software that was opened to begin preparing the protein/ligand files and serves as the UI for the entire operation. This program provides a means to execute AutoDock Vina and was installed in the same file location as Vina.

PyMOL allows the protein and docked ligand to be viewed in 3D. No installation folder required.

Spartan Molecular Modeling software (Student Edition v.9) was used to create the oxygenated buckminsterfullerene structures and convert them to pdb files for use in AutoDock.

Hardware:

AutoDock Vina utilizes all the CPU cores available on the system to perform the docking. The following central processing unit was used for this study:

12th Gen Intel(R) Core (TM) i7-12700K, 3610 Mhz, 12 Core(s), 20 Logical Processor(s)

Installing the Software:

AutoDock MGL Tools was installed to a new folder on the main drive (C:\). For this work, a "Software" folder was created directly onto the C:\ drive. After AutoDock Tools was installed, AutoDock Vina was installed to the AutoDock Tools folder within Software. Files used in AutoDock Tools were kept together in one folder to minimize error. A "Workspace" folder was created to accommodate this. The Workspace folder has all the pdb files and any files generated during the docking process. It also contains a copy of the .exe file for AutoDock Vina.

Acquiring pdb Files:

For this work, a crystallographic structure of the HIV-PR (5CON) obtained from The Brookhaven Protein Data Bank was used to ensure the desired experiments could be performed

successfully. 5CON was chosen as it is wild-type protease, and this would better simulate real life treatment of the virus. The docking method described here was kept constant throughout all the experiments that used the HIV-PR and C₆₀O_x. The ligand that came bound to the 5CON crystal structure (GRL-015) was removed during docking preparation to make room for the molecule being docked. The ligands used to study the HIV-PR were created in Spartan and converted to pdb files within Spartan. All pdb files were placed into the Workspace folder. The startup directory path for AutoDock Tools was set to the Workspace folder.

Preparation For Docking:

Once the pdb file was selected and opened in AutoDock Tools, the protein was prepared by removing unnecessary atoms and adding proper charges. First, all water molecules were removed. It is a frequent practice in docking procedures to remove water molecules from a crystallographic structure as they are rarely involved in the binding process. Depending on how the crystal structure was created and modeled, the water molecules may not even be modeled correctly and will only make it more difficult for AutoDock to perform binding and scoring calculations. This can lead to inaccuracies in docking poses and binding affinity calculations.²⁰ Some works include water and study the interactions it has on protein-ligand interaction, but that is not within the aim of the present study.^{4,21} Next, the ligand that was already bound to the protease (GRL-015) was removed. Afterwards, hydrogens (only polar hydrogens) were added to 5CON. Adding polar hydrogens helps produce accurate ionization data by accounting for deprotonation during the crystallization process of the protein to better simulate the protein's *in-vivo* state.²² At this point, the protein is ready for charges. Assigning accurate charges to a protein structure is a crucial factor in the production of accurate binding simulations.²³ Charges were added in the form of Kollman charges. Kollman charges derive their values from electrostatic potential measurements of each amino acid within the protein structure. At this stage, the protein could be saved to the Workspace folder as a pdbqt file. The pdbqt file format is AutoDock's version of a pdb file that includes the charges designated to the molecule. The prior setup is important for gaining an accurate charge value with respect to the experiment being performed. For the ligand file, the same preparation steps were taken. One key difference in ligand preparation is the ability to select rotatable bonds/torsions within the ligand. AutoDock Tools selects rotatable bonds by default, and these default selections were kept for this run. At

this point, the program must be told where to dock the ligand. The “Grid Box” function of AutoDock Tools provides a 3-dimensional box with adjustable length, width, and height (in Angstroms) transposed onto the macromolecule. Within this 3-Dimensional space, the most ideal binding sites and conformations for the ligand are found. Figures 2 and 3 display the HIV-PR in AutoDock Tools without and with the grid box respectively.

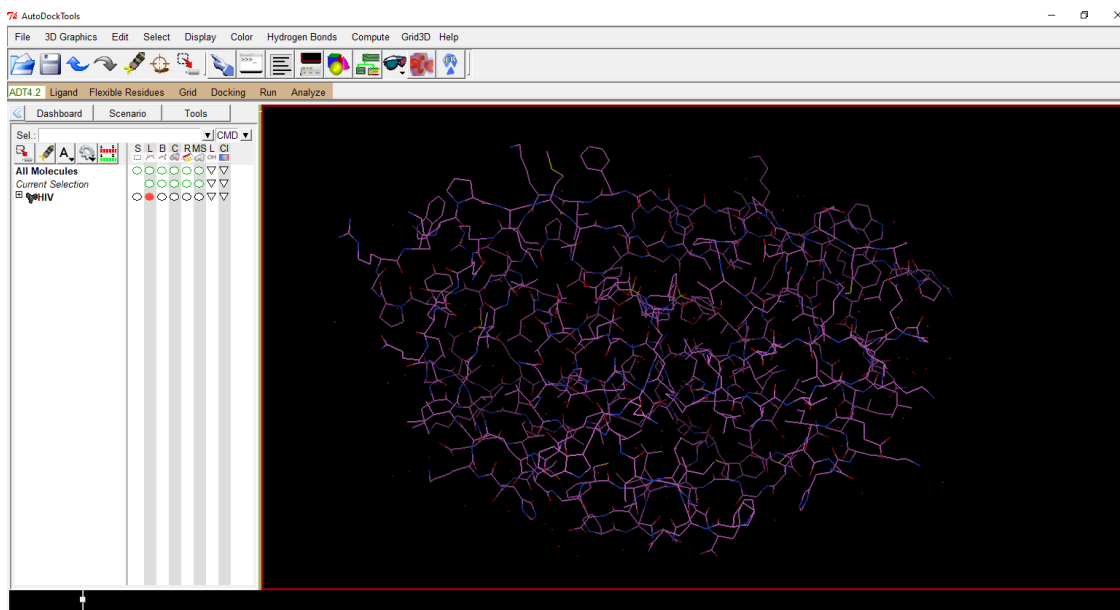


Figure 2: 5CON HIV-PR in AutoDock Tools

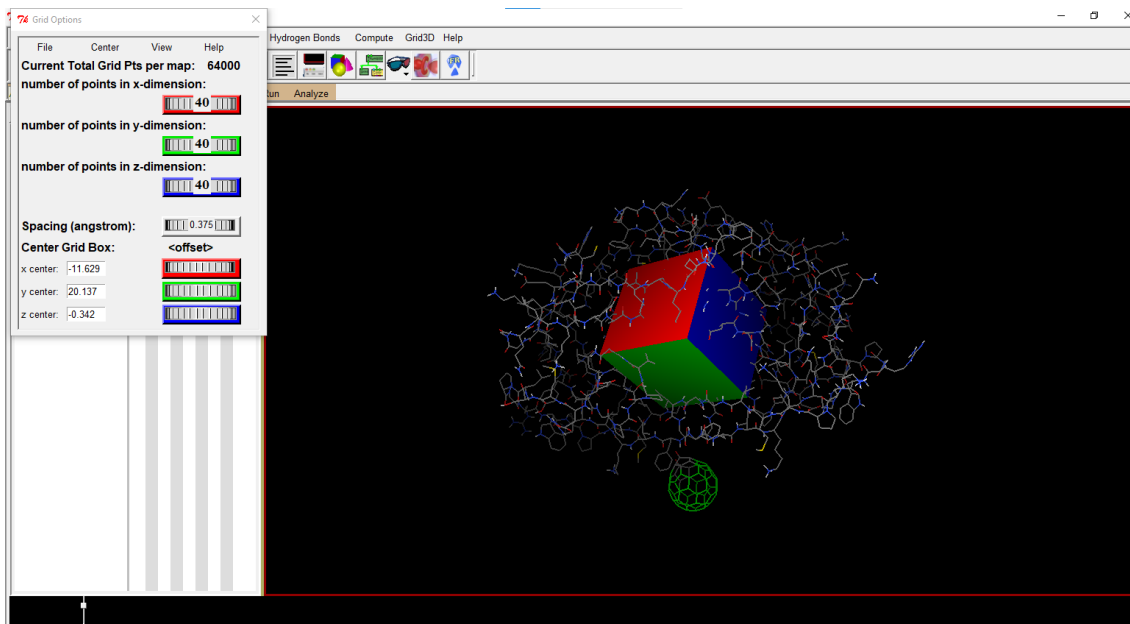
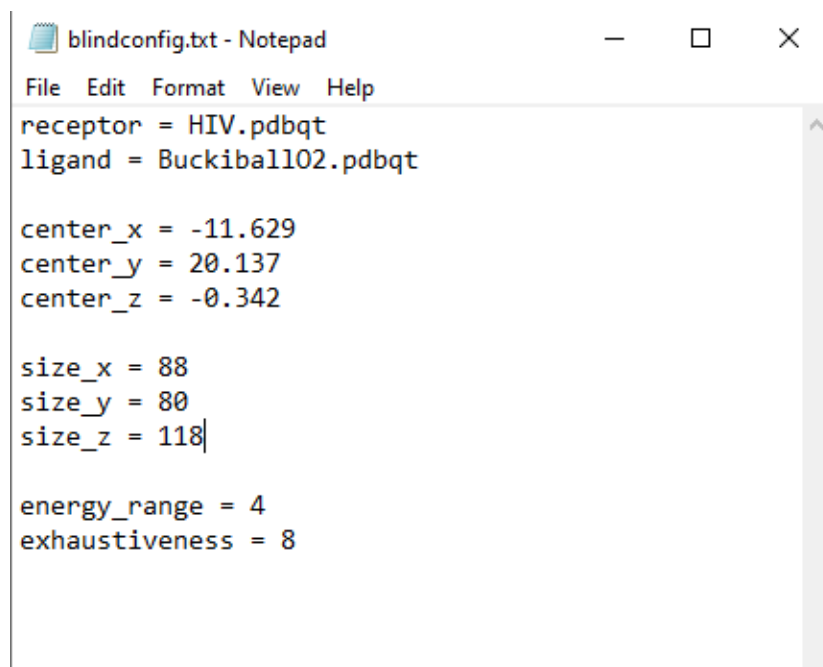


Figure 3: Grid box with adjustable location/size in AutoDock Tools

The active site of a protein can be selected by highlighting the amino acid corresponding to the active site of that macromolecule. If the binding site is not known, it can be found in the literature provided on the page the protein pdb file was downloaded from. Because blind docking was performed in this study, the grid box was not centered around the active site but rather was made to encompass the entire HIV-PR structure. Next, a config.txt file was created in Notepad; AutoDock Vina reads this config file (see Figure 4 below) during the docking process. The formatting is particularly important or else AutoDock Vina will not be able to properly auto-generate the grid map files required for the docking.



```
blindconfig.txt - Notepad
File Edit Format View Help
receptor = HIV.pdbqt
ligand = Buckiball102.pdbqt

center_x = -11.629
center_y = 20.137
center_z = -0.342

size_x = 88
size_y = 80
size_z = 118|

energy_range = 4
exhaustiveness = 8
```

Figure 4: Configuration file for docking

Within the config.txt file, the protein pdbqt file was set as the receptor while the respective ligand pdbqt file is set as the ligand. The coordinates and size parameters of the grid box were input (the size and center locations are measured in grid points that are 0.375Å in length), and energy range and exhaustiveness were kept at their respective default values (4 and 8). Energy range determines the range of binding affinities displayed for the nine conformations in the log file in -kcal/mol. Outliers of this range are not displayed in the log file. Exhaustiveness is a metric for the number of calculations performed during the docking at each step, with accuracy and computational processing requirements increasing linearly with one another. Docking

accuracy becomes notably poor with exhaustiveness < 8 but is sufficient at the default value.²⁴ After prepping the config.txt file, the docking was performed by running AutoDock Vina via command prompt. The current directory was set to the workspace folder via the following command:

```
“cd C:\Softwares\AutoDockTools\Workspace”
```

From here, the following was typed:

```
"C:\Softwares\AutoDockTools\Workspace\vina.exe" --receptor HIV.pdbqt --BuckiballO2.pdbqt -  
-config config.txt --log log.txt --out output.pdbqt.” Following the words “receptor,” “ligand,”  
“config”, “log”, and “out” within the command the specific name of the file respective to those  
titles within the Workspace folder must be used. The log and output (out) files are generated  
during the docking and placed within the Workspace folder. The provided names in the  
command are what the files will be called, meaning that the only restriction upon their names is  
that they do not share a name with an already existing file within the folder. Figure 5 displays an  
example of the command prompt screen following a successful docking command.
```

```
C:\Softwares\AutoDockTools\Workspace>"C:\Softwares\AutoDockTools\Workspac  
t.pdbqt  
#####  
# If you used AutoDock Vina in your work, please cite:  
#  
# O. Trott, A. J. Olson,  
# AutoDock Vina: improving the speed and accuracy of docking  
# with a new scoring function, efficient optimization and  
# multithreading, Journal of Computational Chemistry 31 (2010)  
# 455-461  
# DOI 10.1002/jcc.21334  
# Please see http://vina.scripps.edu for more information.  
#####  
WARNING: The search space volume > 27000 Angstrom^3 (See FAQ)  
Detected 20 CPUs  
WARNING: at low exhaustiveness, it may be impossible to utilize all CPUs  
Reading input ... done.  
Setting up the scoring function ... done.  
Analyzing the binding site ... done.  
Using random seed: 419757624  
Performing search ...  
0% 10 20 30 40 50 60 70 80 90 100%  
|----|----|----|----|----|----|----|----|----|  
*****  
done.  
Refining results ... done.  
  
mode | affinity | dist from best mode  
| (kcal/mol) | rmsd l.b. | rmsd u.b.  
-----  
1 | -9.4 | 0.000 | 0.000  
2 | -9.2 | 15.466 | 18.849  
3 | -8.9 | 15.748 | 19.455  
4 | -8.9 | 0.878 | 3.728  
5 | -8.8 | 1.884 | 6.131  
6 | -8.6 | 26.477 | 30.053  
7 | -8.6 | 16.056 | 19.495  
8 | -8.6 | 26.502 | 30.097  
9 | -8.5 | 26.699 | 30.299  
Writing output ... done.  
C:\Softwares\AutoDockTools\Workspace>
```

Figure 5: Command Prompt of Executed Docking For Trial Run

Output and Log Files

Upon executing the command, the docking simulations are run, and two files are produced: the log.txt file (see Figure 6 below), and the output.pdbqt file. The log file is simply a text document that displays information obtained from AutoDock Vina's scoring function (also viewable within command prompt where the command was entered and executed). The generated table lists the binding affinities for each docking pose in -kcal/mol released, so a lower value indicates a more stable conformation (ex. -9.0 kcal/mol is more stable than -8.0 kcal/mol). The log file also provides values for Root Mean Square Deviation lower and upper bound (RMSD l.b and RMSD u.b respectively). These values examine the distances the atoms move from the most stable conformation (the first docking pose). Naturally, the RMSD values for the first docking pose are 0.000 because they are calibrated around that pose. More specifically, the upper bound parameter examines the distance moved for each of the same exact atoms in conformer 1 vs the other. The lower bound matches each atom in one conformation with the same type of atom in the other conformation to get the most ideal theoretical value. As a result, the lower bound values will be lower. Both RMSD calculations are presented in Angstroms and factor in atoms that are not hydrogen.

```
File Edit Format View Help
#####
# If you used AutoDock Vina in your work, please cite:      #
#                                                           #
# O. Trott, A. J. Olson,                                    #
# AutoDock Vina: improving the speed and accuracy of docking #
# with a new scoring function, efficient optimization and    #
# multithreading, Journal of Computational Chemistry 31 (2010) #
# 455-461                                                    #
#                                                           #
# DOI 10.1002/jcc.21334                                     #
#                                                           #
# Please see http://vina.scripps.edu for more information.  #
#####

WARNING: The search space volume > 27000 Angstrom^3 (See FAQ)
Detected 20 CPUs
WARNING: at low exhaustiveness, it may be impossible to utilize all CPUs
Reading input ... done.
Setting up the scoring function ... done.
Analyzing the binding site ... done.
Using random seed: 419757624
Performing search ... done.
Refining results ... done.

mode |  affinity | dist from best mode
      | (kcal/mol) | rmsd l.b. | rmsd u.b.
-----+-----+-----+-----
  1   |    -9.4   |    0.000   |    0.000
  2   |    -9.2   |   15.466   |   18.849
  3   |    -8.9   |   15.748   |   19.455
  4   |    -8.9   |    0.878   |    3.728
  5   |    -8.8   |    1.884   |    6.131
  6   |    -8.6   |   26.477   |   30.053
  7   |    -8.6   |   16.056   |   19.495
  8   |    -8.6   |   26.502   |   30.097
  9   |    -8.5   |   26.699   |   30.299
Writing output ... done.
```

Figure 6: Docking Log file Output Example

Making Oxygenated C₆₀ In Spartan

After ensuring the program could successfully simulate docking, the next step was to create an oxygenated buckminsterfullerene ligand to use on an HIV-PR. This was achieved in Spartan according to the following steps:

First, a five membered ring of sp² carbons with conjugated double bonds is created as depicted in Figure 7a below.

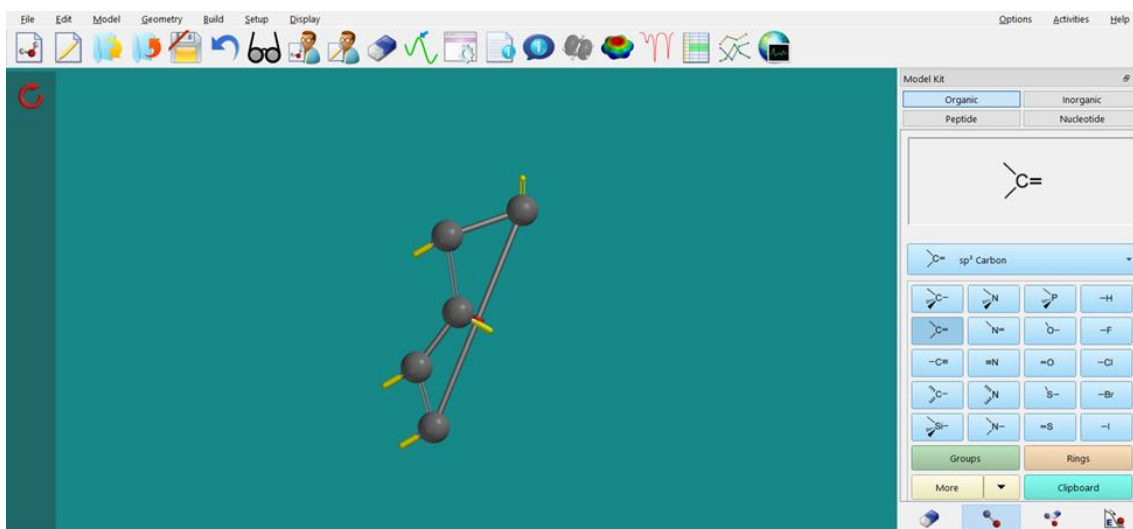


Figure 7a: Base ring for buckminsterfullerene

The energy was then minimized to simplify the shape. Five copies were made of the depicted ring structure and arranged as follows in Figure 7b:

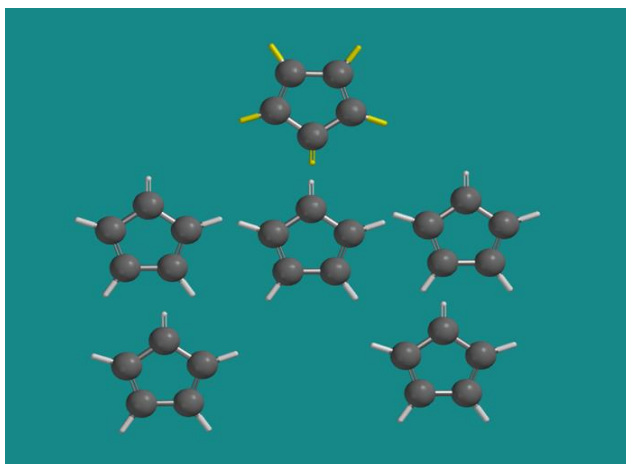


Figure 7b: Six rings that will form C₃₀

The rings were then connected as such in Figure 7c

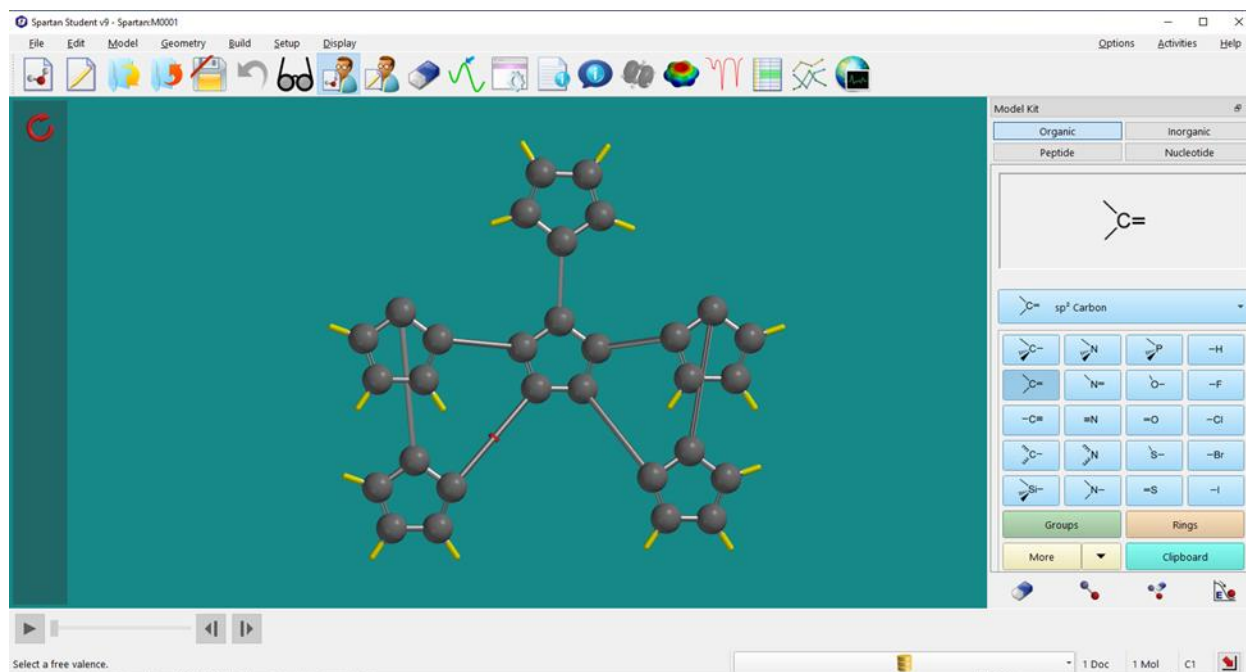


Figure 7c: Connected C₅ rings

After minimizing the energy, three six membered rings were formed by connecting the available valences (shown in Figure 7d) to finish the C₃₀.

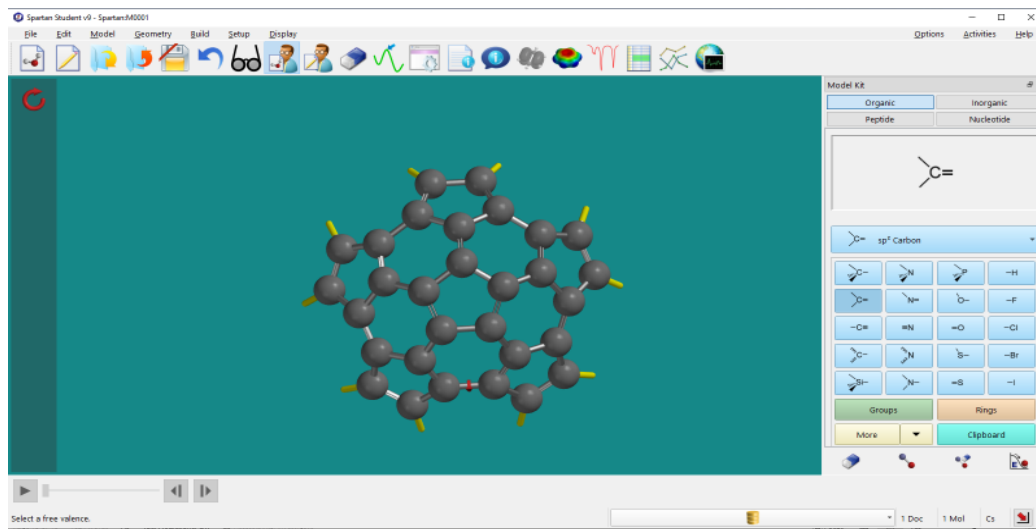


Figure 7d: C₃₀ Ring

A copy of the C₃₀ depicted in Figure 7d was made and positioned above the other. Valences were connected as follows in Figure 7e:

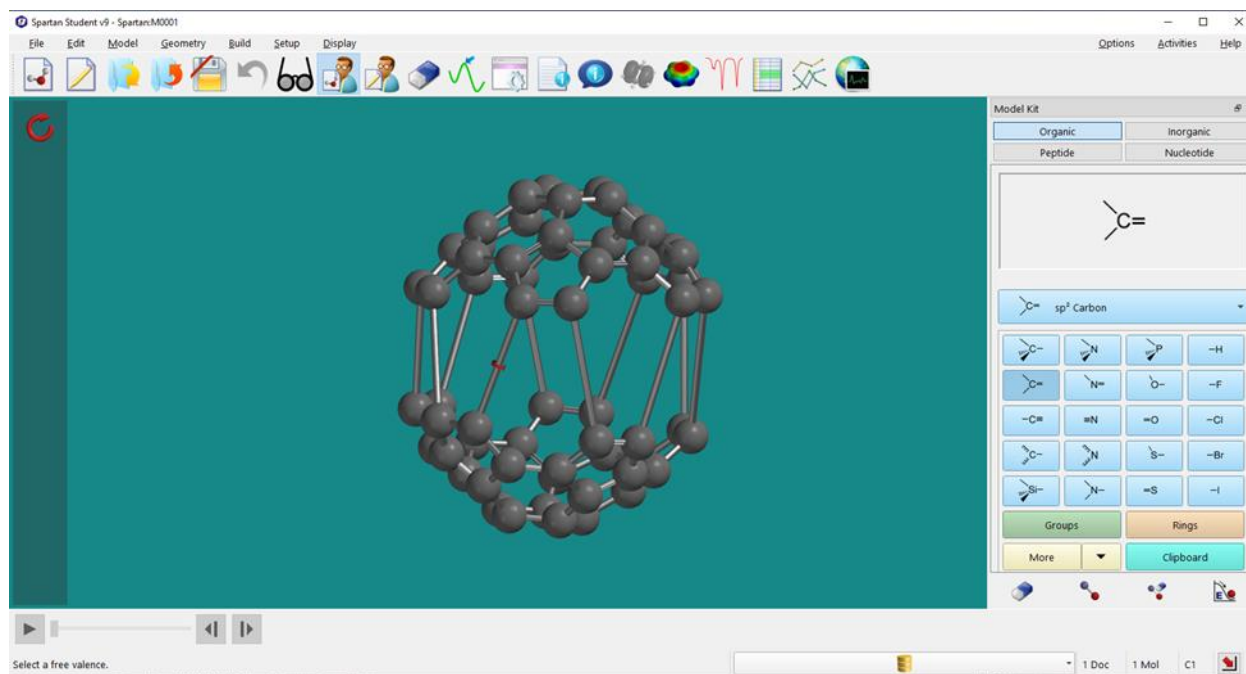


Figure 7e: Connected C30s.

The energy was minimized to create a proper buckminsterfullerene structure. To make this buckyball oxygenated, a double bond was deleted between two of the six membered rings and two carbonyl groups were bonded in place of the new valences as seen in Figure 7f.

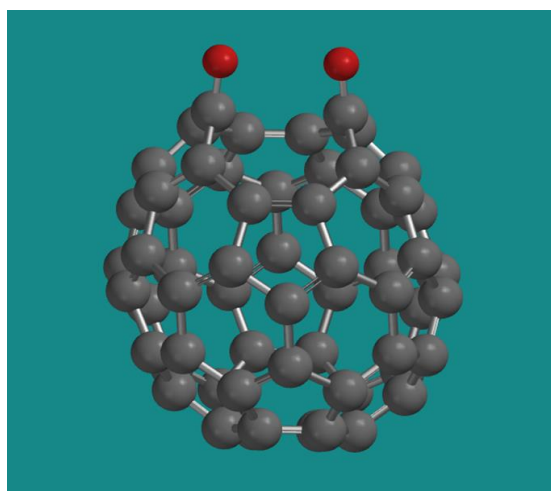


Figure 7f: C₆₀O₂ model in Spartan Software

When saving the newly created C₆₀ model, the file extension must be changed from “.spartan” to “.pdb” for Windows to be able to read the 3D model as a pdb file usable within AutoDock Vina.

Electrostatic Potential Map in Spartan

Spartan features an electrostatic potential map that displays the localized valences for all locations across the surface of the molecule's structure. This tool was used to make the alternate structures of $C_{60}O_{4-12}$ (described in the **Goals and Objectives** section). C_{60} is a symmetrical structure with no dipole moments giving rise to any notable differences in electrostatic potential. However, the oxygenated variants of C_{60} used in this study have extraordinarily strong dipole moments around the electronegative oxygen atoms in the present carbonyls. This creates slightly negative charges at the oxygen atoms and a resulting electrophilic zone at the base of these carbonyls. The electrostatic map in Spartan was created via surface calculations with the following parameters: Equilibrium geometry in gas phase with PM3. Initially the plan was to calculate the equilibrium geometry in gas with density function using ω B97X-D and 6-31G*, but C_{60} has too many atoms for the Spartan to perform these calculations. Clicking any point on the molecule's electrostatic potential map displays the electron valence energy in kilojoules. Visually, electropositive sections are displayed in blue and electronegative in red (with green being in the center, see Figure 8), but since the molecule is mostly carbon atoms, the valence varies little aside from the oxygens which are very electronegative. To get a better visualization of the electrostatic variance in the molecule, the lower and upper bounds for the valence energy were reduced from ± 200 kJ to ± 20 kJ. Setting the valence energy boundaries to ± 20 kJ made it much easier to see the electropositive and electronegative regions on the $C_{60}O_x$ structures. Using this data, a double bond in a highly positive region (indicated by a high valence energy) would be chosen as the site for additional carbonyl groups added in the $C_{60}O_{4-12}$ structures as depicted in the transition from Figure 8 to Figure 9.

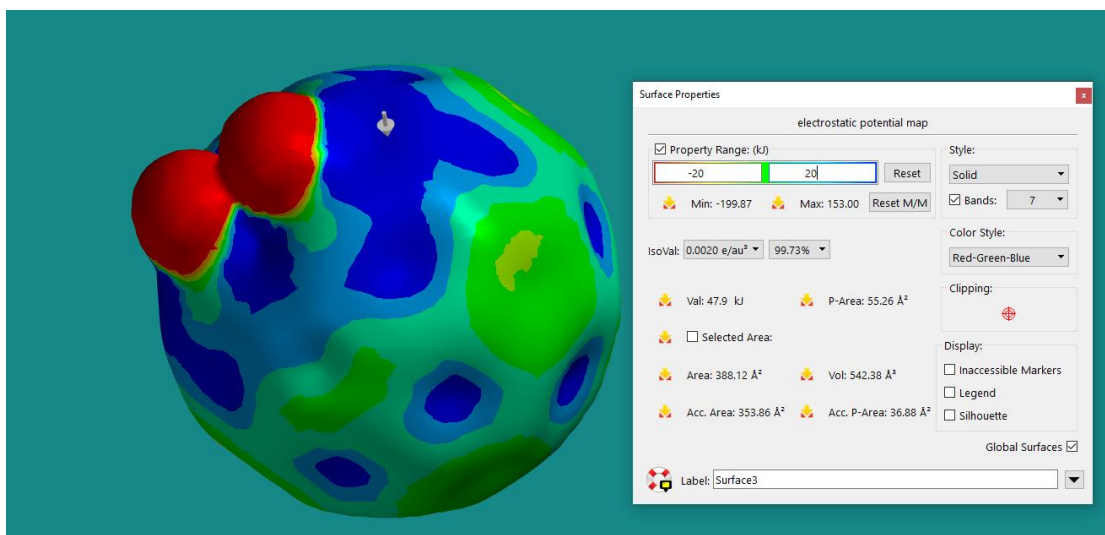


Figure 8: Electrostatic potential map for $C_{60}O_2$ with modified energy boundaries

Once the electrophilic zone was identified, the double bond at that site was removed (mimicking an ozonolysis reaction) and two carbonyls were added to create the corresponding “E” structure.

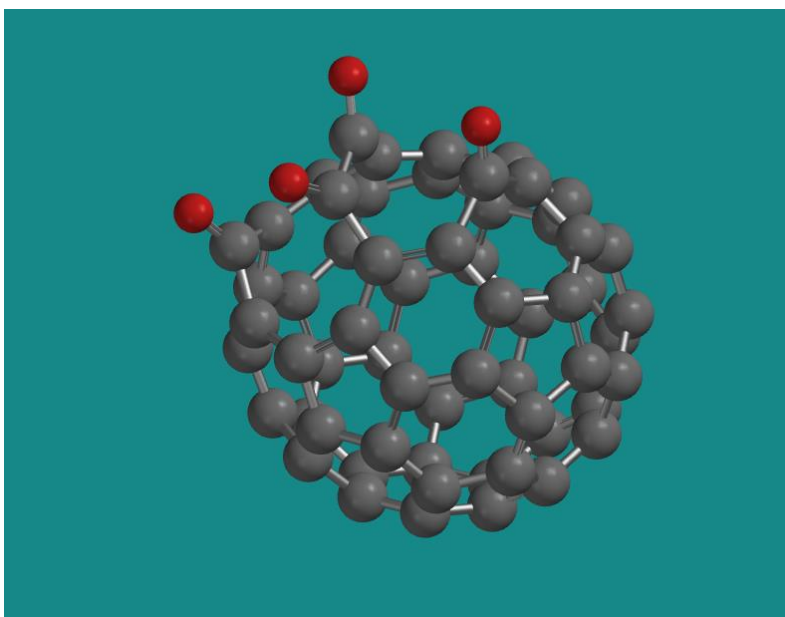


Figure 9: $C_{60}O_4$ -E created by placing carbonyls at electrophilic sites

HIV-Protease Docking Analysis with PyMol

Opening the HIV pdbqt file in PyMol brings up the following screen:

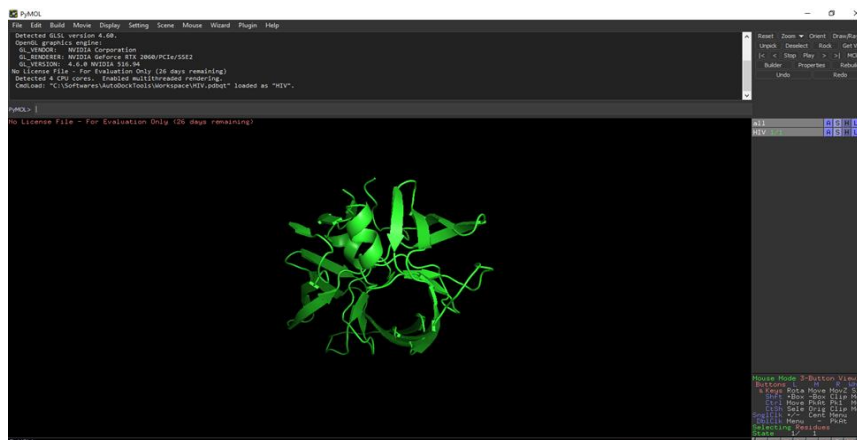


Figure 10: HIV-PR ribbon form in PyMOL

By default, the protein will appear in a ribbon structure as seen in Figure 10. For this experiment, the surface and stick structure displays were used for viewing docking interactions. The output file generated from the docking was opened in PyMOL alongside the protein pdbqt file. This places the ligand at the binding site discovered by AutoDock Vina on the protein. The arrow keys can be used to cycle through the different conformations of the binding that are detailed in the generated log file. To understand how the oxygenated fullerene compounds interact with the residues of the HIV-PR during the docking processes, the hydrogen bonding locations and distances were viewed within PyMOL. Trying to examine where the hydrogen bonds are with the entire HIV-PR present is cumbersome. This was fixed by first hiding the entire HIV structure, and then using the command, “show sticks, byres all within 5 of *ligand name*”. This will only display the amino acid residues within 5 angstroms of the ligand in each docking pose. Hydrogen bonds are typically 2.7Å-3.3Å which is well within the 5Å radius. The amino acid residues that the protein is composed of are displayed in a sequence in PyMOL. Each amino acid is displayed via its one letter code, and clicking an amino acid on the protease structure highlights the residue in the list, and clicking the residue from the list will highlight it in the display (provided that amino acid is not hidden). Using this feature, the residues that have hydrogen bonding with the docked C₆₀O_X structures were easily identifiable with each conformation. Next, the hydrogen bonds were displayed as yellow dashed lines via “Find Polar

Contacts” with the “Action” command on the ligand’s profile in PyMOL. After generating the hydrogen bond lines, the distances of those bonds were calculated using the “Measurement” command within the “Wizard” function in PyMOL (shown in Figure 11). This command displays the distances of the polar contacts in angstroms for all hydrogen bonds in all docking poses.

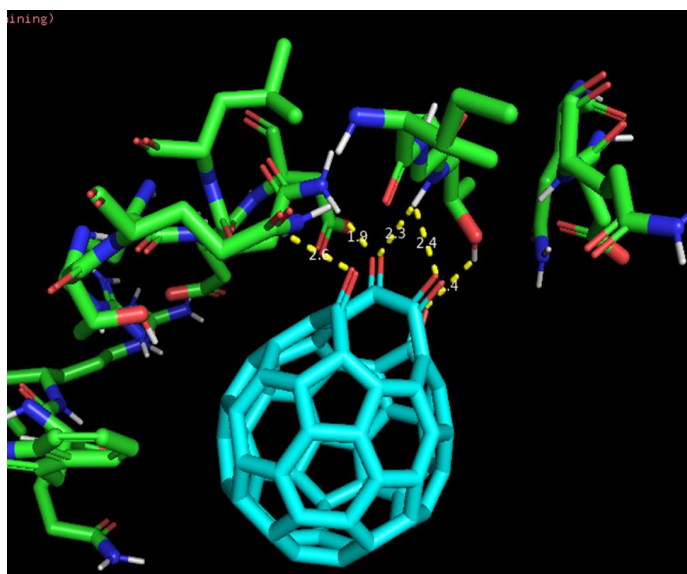


Figure 11: PyMOL analysis of H-bonds between C₆₀O₄ and HIV-PR residues

Using the above methods, eight total C₆₀O_x structures were created and docked. Table 1 lists every structure that was docked in this experiment.

Table 1: The C₆₀O_x structures studied and documented

Structure	Oxygen Position
C ₆₀ O	N/A
C ₆₀ O ₂	N/A
C ₆₀ O ₄ -G	Geometrical
C ₆₀ O ₄ -E	Electrostatic
C ₆₀ O ₆ -G	Geometrical
C ₆₀ O ₆ -E	Electrostatic
C ₆₀ O ₈ -G	Geometrical
C ₆₀ O ₈ -E	Electrostatic

The order of display for each structure goes from the smallest number of oxygens present (1 in C₆₀O) to the largest number (C₆₀O₈). Results for C₆₀O_x-G structures based on geometric stability were displayed first, followed by C₆₀O_x-E structures based on electrostatic stability (see page 7 under Goals and Objectives for difference between G and E structures). The strongest bonding exhibited in the docking process is hydrogen bonding. The location and length of the hydrogen bonds in each docking conformation elucidates the location of the preferred binding sites. To better understand the HIV-PR and C₆₀O_x interactions, the H-bonds formed by each conformation were closely examined and documented. One docking simulation for each compound was detailed in the following section each with a table that includes the following data: Binding affinity (from the generated log files for each run), hydrogen bond location (to which residues), and hydrogen bond length. Oxygens are arbitrarily assigned numbers within each figure to provide a frame of reference for the binding data in the tables. Following C₆₀O₄-G, the number of residues displayed in each image is reduced to only those with H-bonds as the increased amount of H-bonds begins to make the screenshots cluttered. The terms “docking pose” and “conformation” are used interchangeably to describe each screenshot analyzed within each ligand’s docking results.

RESULTS:

C₆₀O

Table 2: C₆₀O Docking Results

Docking Pose	Affinity (kcal/mol)	H Bond Location	H Bond Distance	Comments
1	-9.0	N/A		No H bond
2	-8.7	N/A		No H bond
3	-8.7	O-Leu-10A	2.7	
4	-8.7	O-Thr-74B	2.4	
5	-8.6	N/A		No H bond
6	-8.5	N/A		No H bond
7	-8.5	O-Thr-74B	2.3	
8	-8.3	O-Leu-10A	2.5	
9	-8.3	N/A		No H bond

Table 2 details the binding affinity and H-bonds of each docking conformation for C₆₀O. Kumar's characterization of the synthesized C₆₀O_x structures through FT-IR, ¹³C NMR, and SALI showed evidence of epoxide functionality, indicating the presence of C₆₀O molecules within the batch mixture. Therefore, a structure for C₆₀O was tested. Compared to C₆₀O₂₋₈ structures, C₆₀O displayed the weakest binding affinity with its most stable conformation at -9.0 kcal/mol. This structure also displays the fewest hydrogen bonds (4). Figure 12 displays the surface area view of the entire HIV-PR with C₆₀O, and figures 12a-i show the docking results for C₆₀O at Leu-10A and Thr-74B achieved through blind docking. Despite the high binding energy seen in some conformations (particularly poses 1 and 2, Figures 12a and 12b), no hydrogen bonding is observed, indicating the presence of strong dipole-dipole and van der waals interactions.

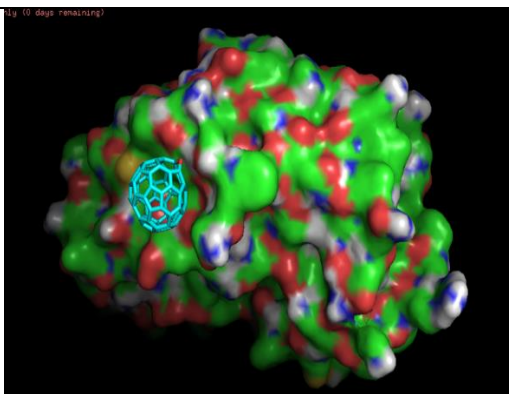


Figure 12: Surface area display of HIV-PR in PyMOL with pose C₆₀O 1

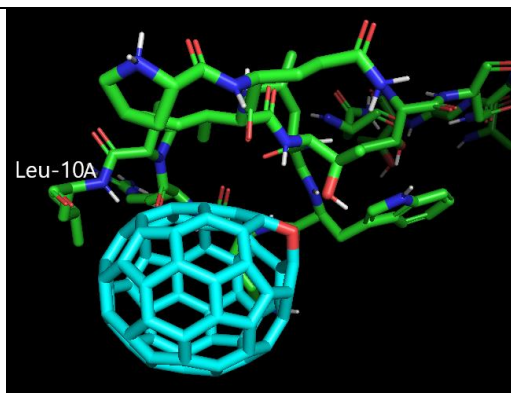


Figure 12a: C₆₀O conformation 1 with the HIV-PR (-9 kcal/mol)

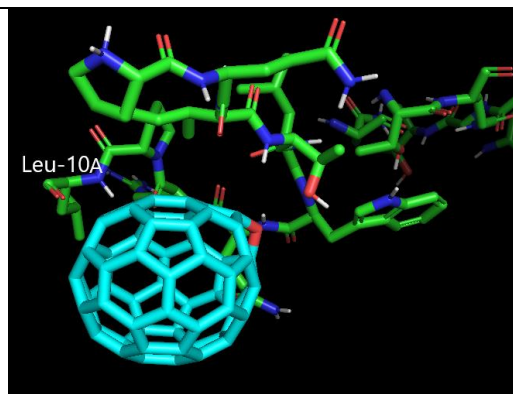


Figure 12b: C₆₀O conformation 2 with the HIV-PR (-8.7 kcal/mol)

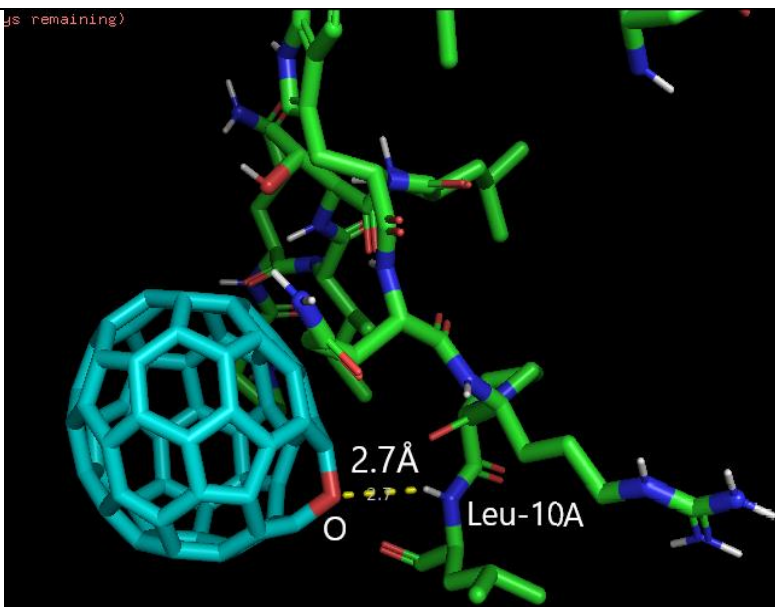


Figure 12c: C₆₀O conformation 3 with the HIV-PR (-8.7 kcal/mol)

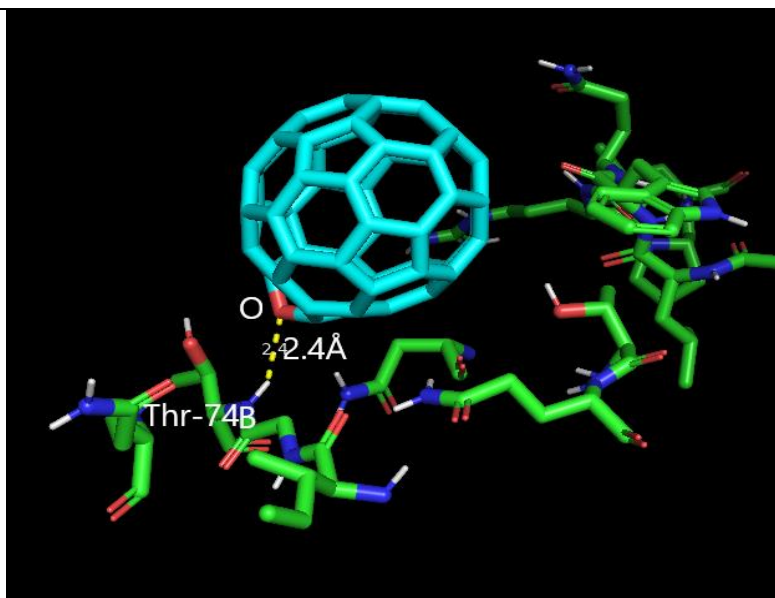


Figure 12d: C₆₀O conformation 4 with the HIV-PR (-8.7 kcal/mol)

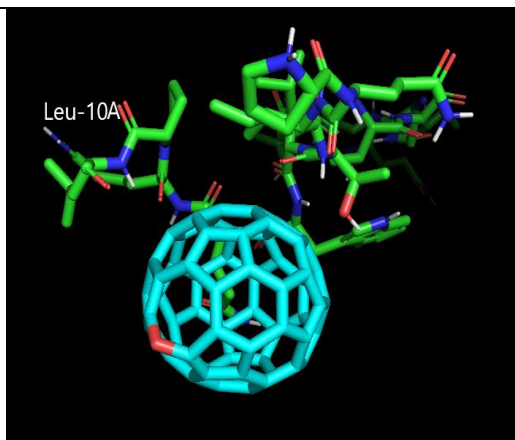


Figure 12e: C₆₀O conformation 5 with the HIV-PR (-8.6 kcal/mol)

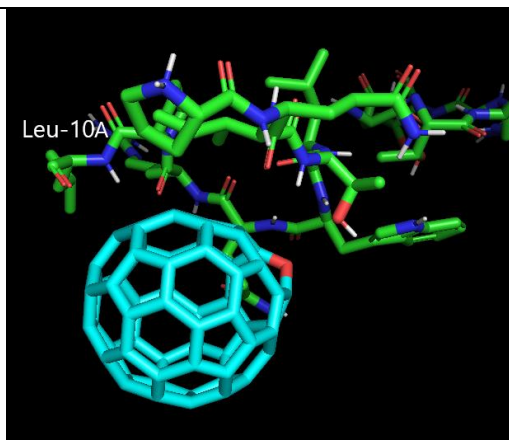


Figure 12f: C₆₀O conformation 6 with the HIV-PR (-8.5 kcal/mol)

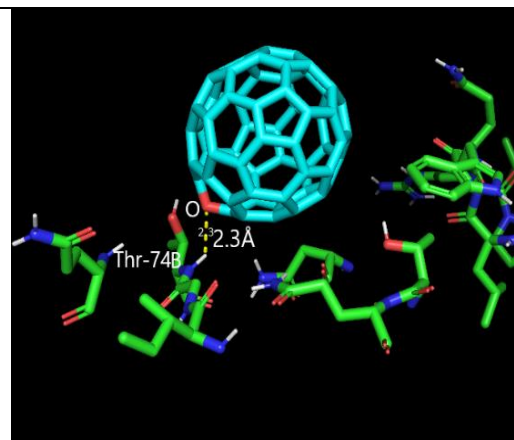


Figure 12g: C₆₀O conformation 7 with the HIV-PR (-8.5 kcal/mol)

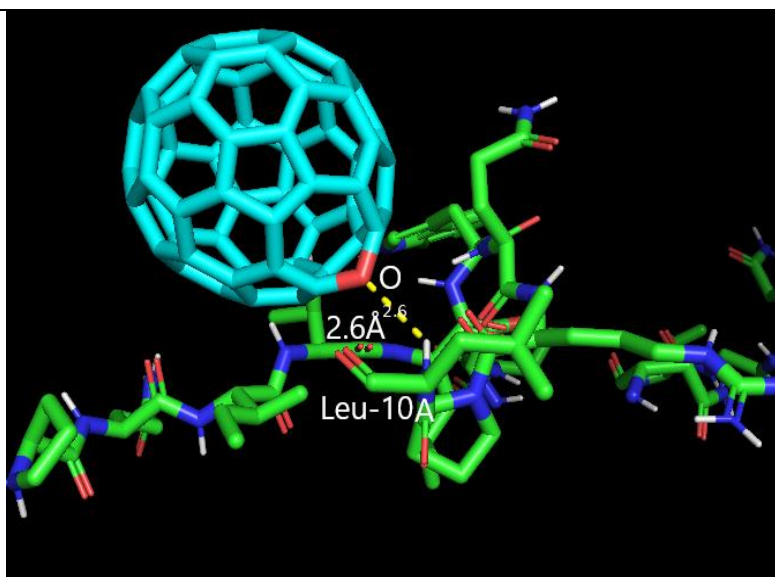


Figure 12h: C₆₀O conformation 8 with the HIV-PR (-8.3 kcal/mol)

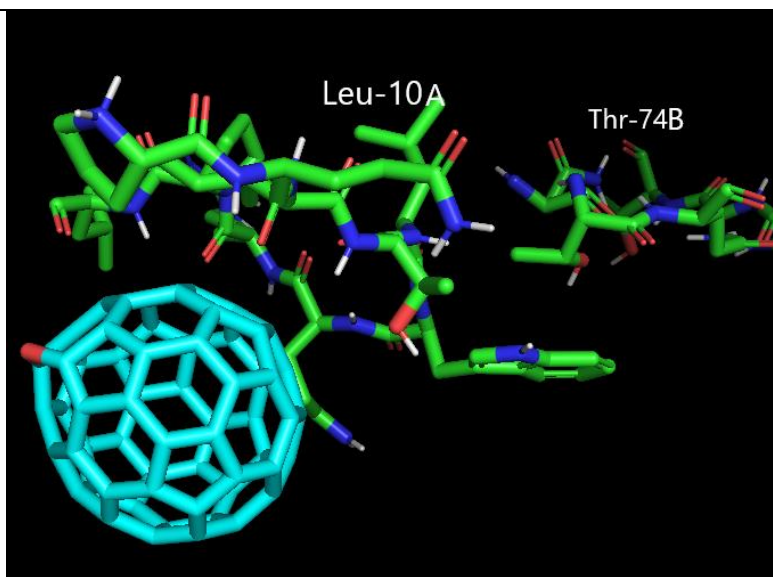


Figure 12i: C₆₀O conformation 9 with the HIV-PR (-8.3 kcal/mol)

C₆₀O₂

Table 3: C₆₀O₂ Docking Results

Docking Poses	Affinity (kcal/mol)	H Bond Location	H Bond Distance (Å)	Comments
1	-9.4	O.1-Thr-4A O.2-Thr-4A	2.1, 2.6	O.1 and O.2 bonded to two different H atoms on Thr-4
2	-9.2	O.1-Thr-4A	1.9	
3	-9.1	O.2-Thr-4A	2.6	
4	-9.0	O.1-Asn-88B O.1-Thr-74B O.2-Thr-74B	2.2, 1.8, 2.5	O.1 and O.2 bonded to two different H atoms on Thr-74
5	-8.8	O.1-Asn-88B O.1-Thr-74B O.2-Thr-74B	2.2, 2.1, 2.5	
6	-8.8	N/A		No H bond
7	-8.8	O.2-Thr-4A	2.1	
8	-8.8	N/A		No H bond
9	-8.8	N/A		No H bond

Table 3 has the binding affinity and H-bonds of each docking conformation for C₆₀O₂. C₆₀O₁₋₈ was found to have the greatest rates of inhibition in Kumar's experiments, and C₆₀O₂ underwent docking experiments following C₆₀O. Over twice as many H-bonds were observed (11 compared to 4 from C₆₀O). The number of H-bonds is not necessarily indicative of binding strength, as the most stable pose in this set (Figure 13a) has two hydrogen bonds compared to poses 4 and 5 which exhibit 3 H-bonds (Figures 13d and 13e). Poses 1, 2, 3, and 7 (Figures 13a, 13b, 13c, and 13g respectively) all bind at the same site(s) on Thr-4A with minor variations in binding (bond length, atoms bound to etc.) Figure 13 displays the surface area view of the entire HIV-PR with C₆₀O₂, and figures 13a-i show the docking results for C₆₀O₂ at Thr-4A, Asn-88B and Thr-74B achieved through blind docking.

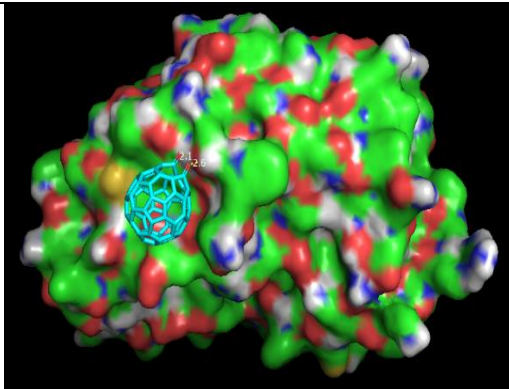


Figure 13: Surface area display of HIV-PR in PyMOL with pose C₆₀O₂ 1

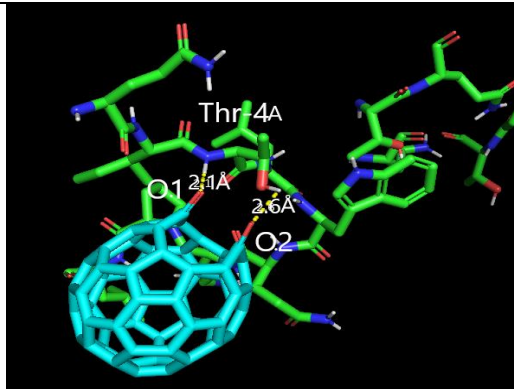


Figure 13a: C₆₀O₂ conformation 1 with the HIV-PR (-9.4 kcal/mol)

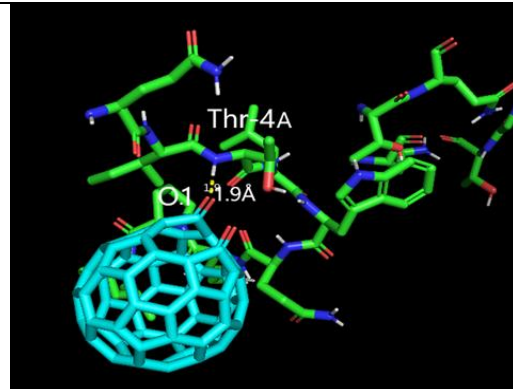


Figure 13b: C₆₀O₂ conformation 2 with the HIV-PR (-9.2 kcal/mol)

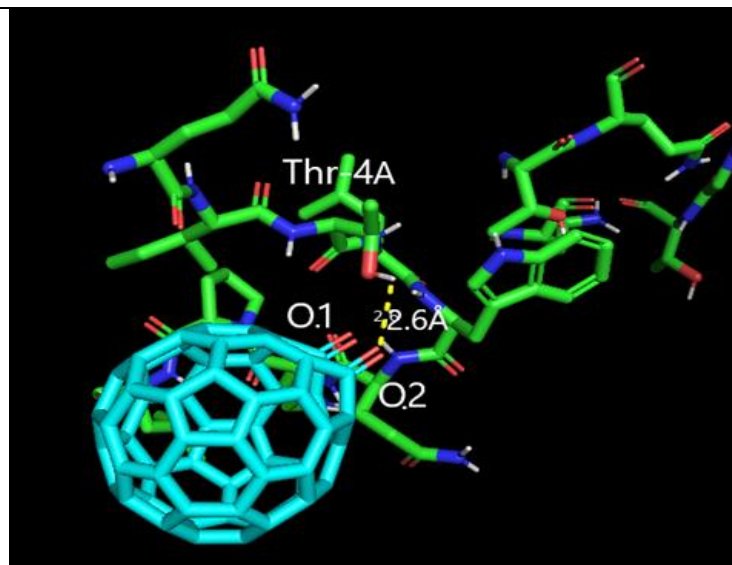


Figure 13c: C₆₀O₂ conformation 3 with the HIV-PR (-9.1 kcal/mol)

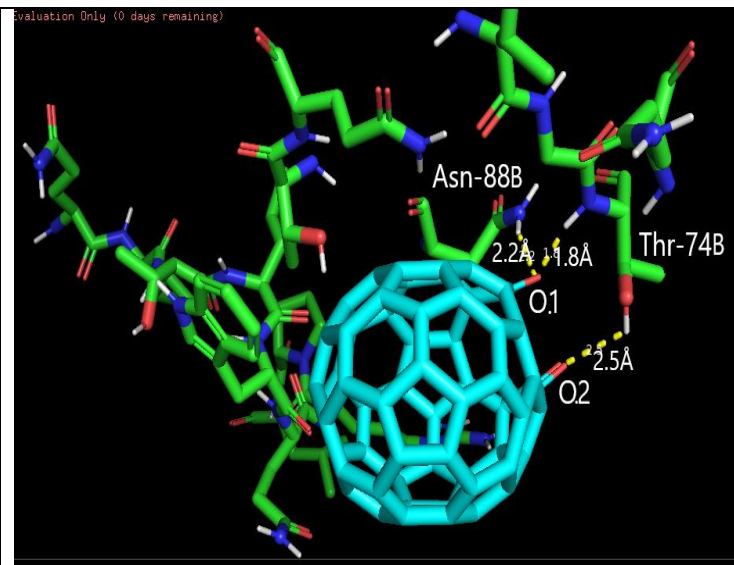


Figure 13d: C₆₀O₂ conformation 4 with the HIV-PR (-9.0 kcal/mol)

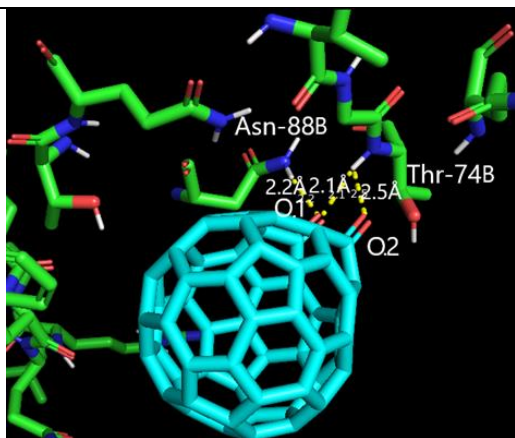


Figure 13e: C₆₀O₂ conformation 5 with the HIV-PR (-8.8 kcal/mol)

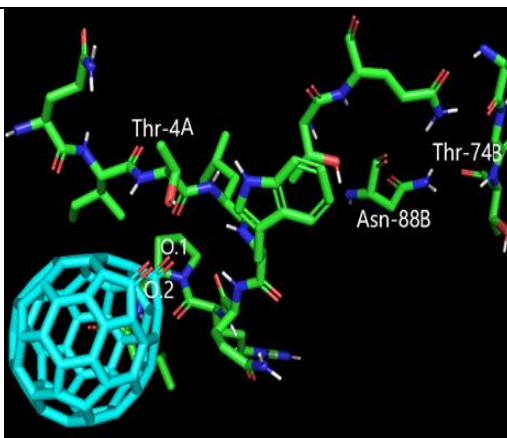


Figure 13f: C₆₀O₂ conformation 6 with the HIV-PR (-8.8 kcal/mol)

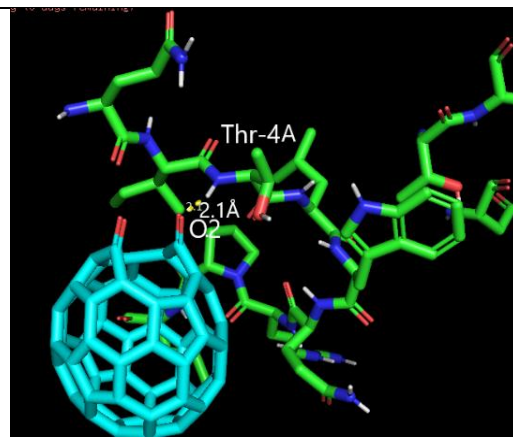


Figure 13g: C₆₀O₂ conformation 7 with the HIV-PR (-8.8 kcal/mol)

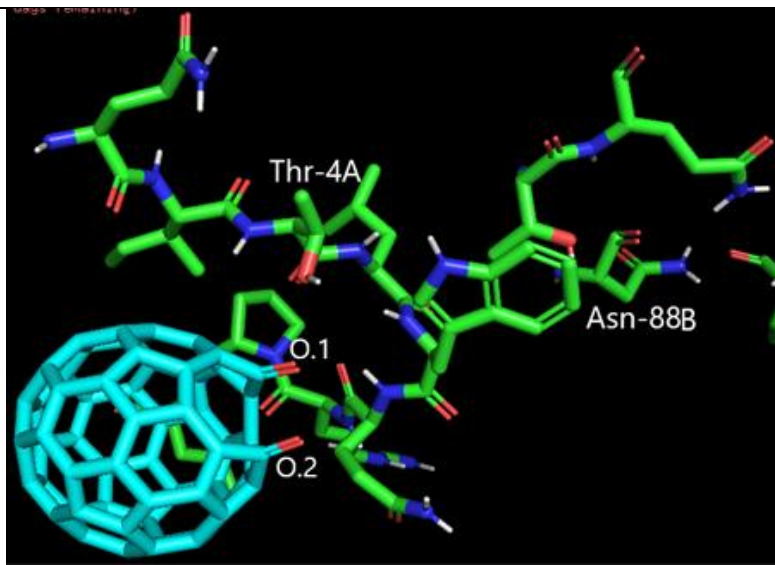


Figure 13h: C₆₀O₂ conformation 8 with the HIV-PR (-8.8 kcal/mol)

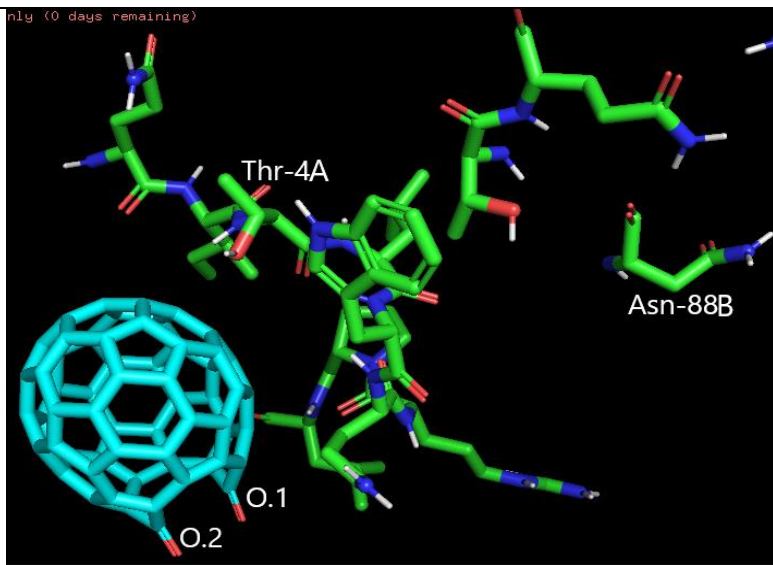


Figure 13i: C₆₀O₂ conformation 9 with the HIV-PR (-8.8 kcal/mol)

C₆₀O₄-G

Table 4: C₆₀O₄-G Docking Results

Docking Poses	Affinity (kcal/mol)	H Bond Location	H Bond Distance (Å)	Comments
1	-9.4	O.1-Thr-4A O.2-Thr-4A	2.2, 2.7	O.1 and O.2 bonded to two different H atoms
2	-9.4	O.1-Thr-4A O.2-Thr-4A	2.2, 2.7	O.1 and O.2 bonded to two different H atoms
3	-9.3	O.1-Asn-88B O.1-Thr-74B O.2-Thr-74B	2.2, 2.1, 2.5	
4	-9.3	O.1-Asn-88B O.1-Thr-74B O.2-Thr-74B	2.2, 2.1, 2.5	
5	-8.9	O.1-Asn-88B O.1-Thr-74B O.2-Thr-74B	2.1, 1.9, 2.4	O.1 and O.2 bonded to two different H atoms on Thr-74
6	-8.9	O.1-Asn-88B O.1-Thr-74B O.2-Thr-74B	2.1, 1.9, 2.4	O.1 and O.2 bonded to two different H atoms on Thr-74
7	-8.9	O.1-Asn-88B O.1-Thr-74B O.2-Thr-74B	2.1, 2.4, 2.4	
8	-8.8	O.1-Thr-74A O.2-Thr-74A O.2-Asn-88A	2.5, 2.1, 2.1	
9	-8.7	N/A		No H bond

Table 4 details the binding affinity and H-bonds of each docking conformation for C₆₀O₄-G. C₆₀O₄-G is the first of two different C₆₀O₄ structures to undergo docking experiments. This version of C₆₀O₄ contains the carbonyls at opposing ends of the structure to maximize stability within the molecule ('G' to denote the structure is based on Geometrical stability), whereas the other structure (C₆₀O₄-E) has the oxygens placed at the most electrophilic sites on the molecule ('E' to denote the carbonyls are assigned based on Electrostatic potential). Interestingly, this docking experiment yielded multiple instances where two conformations were the exact same (poses 1 and 2, 3 and 4, as well as 5 and 6, Figures 14a, 14b, 14c, 14d, 14e, and 14f respectively) indicating a possible lack of varied viable conformations for this structure. These are the docking results for C₆₀O₄-G at Thr-4A, Asn-88A, Asn-88B, Thr-74A and Thr-74B achieved through blind docking displayed in Figures 14, and 14a-i.

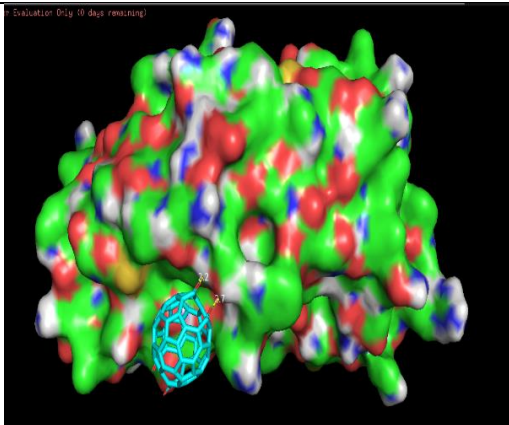


Figure 14: Surface area display of HIV-PR in PyMOL with pose C₆₀O₄-G 1

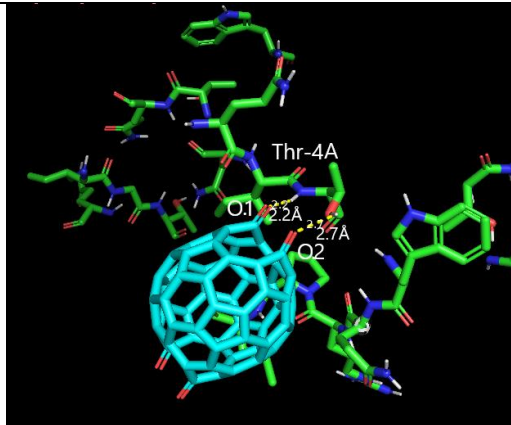


Figure 14a: C₆₀O₄-G conformation 1 with the HIV-PR (-9.4 kcal/mol)

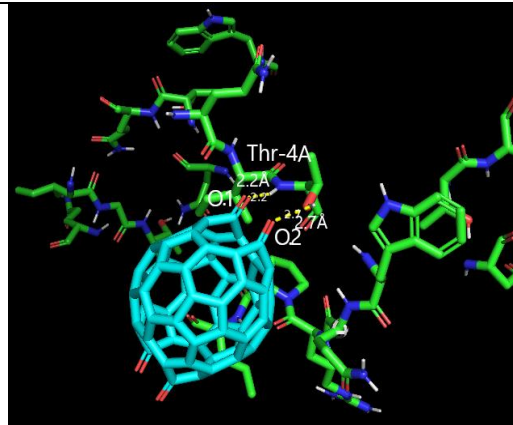


Figure 14b: C₆₀O₄-G conformation 2 with the HIV-PR (-9.4 kcal/mol)

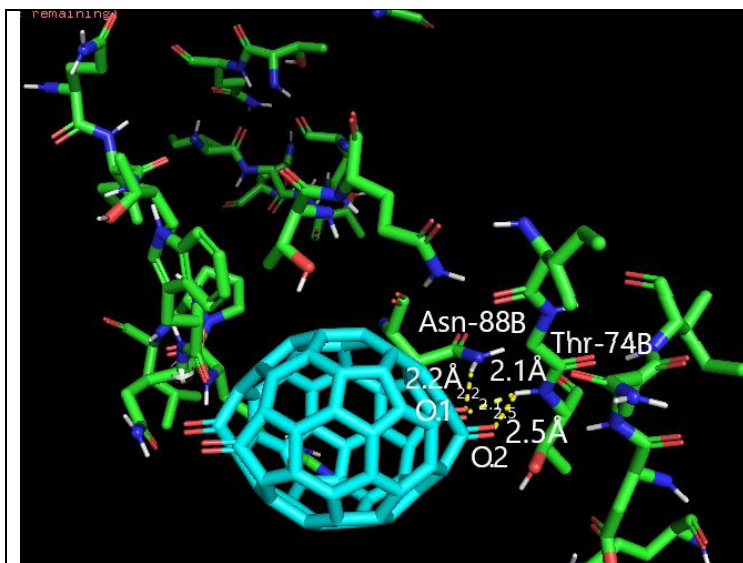


Figure 14c: C₆₀O₄-G conformation 3 with the HIV-PR (-9.3 kcal/mol)

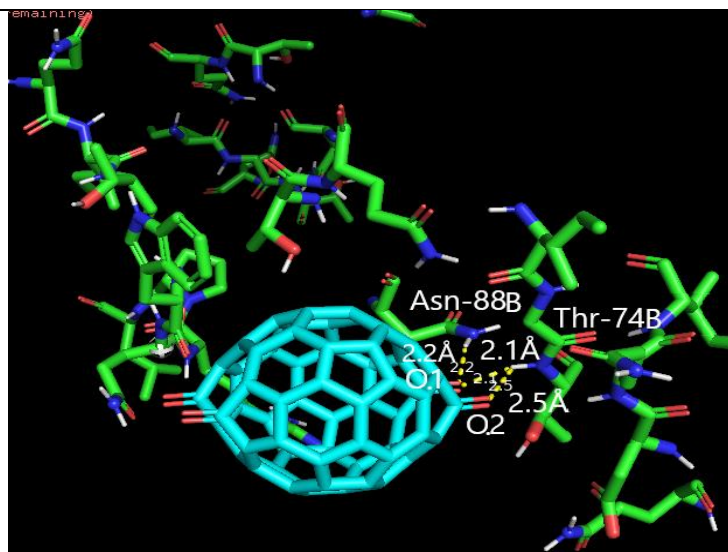


Figure 14d: C₆₀O₄-G conformation 4 with the HIV-PR (-9.3 kcal/mol)

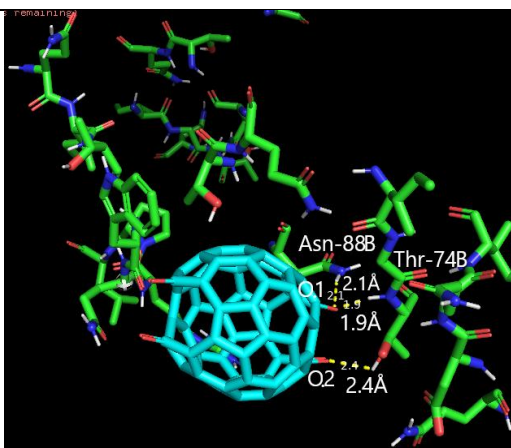


Figure 14e: C₆₀O₄-G conformation 5 with the HIV-PR (-8.9 kcal/mol)

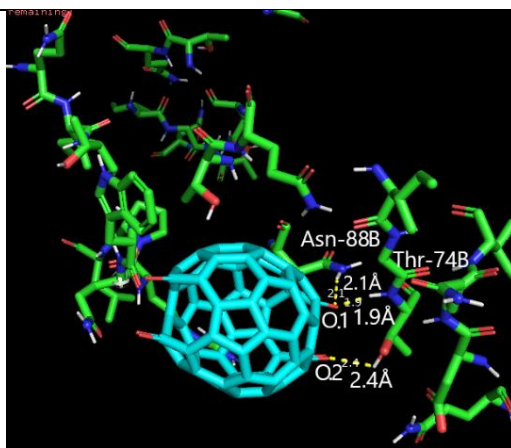


Figure 14f: C₆₀O₄-G conformation 6 with the HIV-PR (-8.9 kcal/mol)

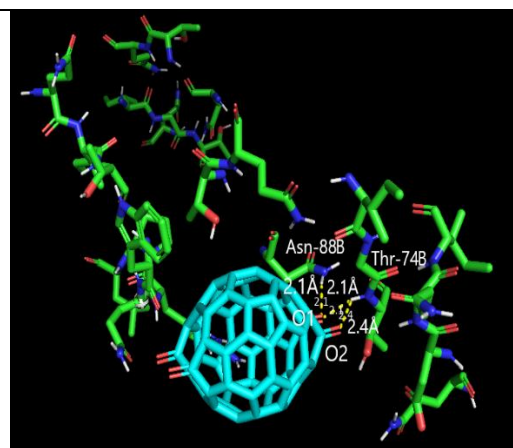


Figure 14g: C₆₀O₄-G conformation 7 with the HIV-PR (-8.9 kcal/mol)

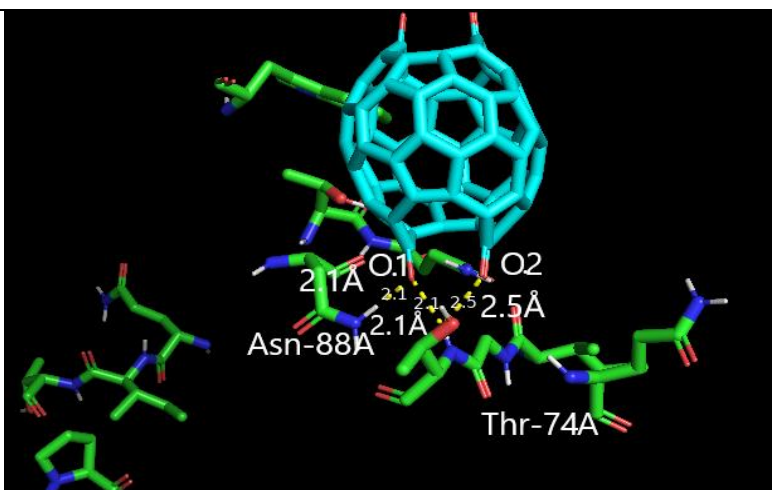


Figure 14h: C₆₀O₄-G conformation 8 with the HIV-PR (-8.8 kcal/mol)

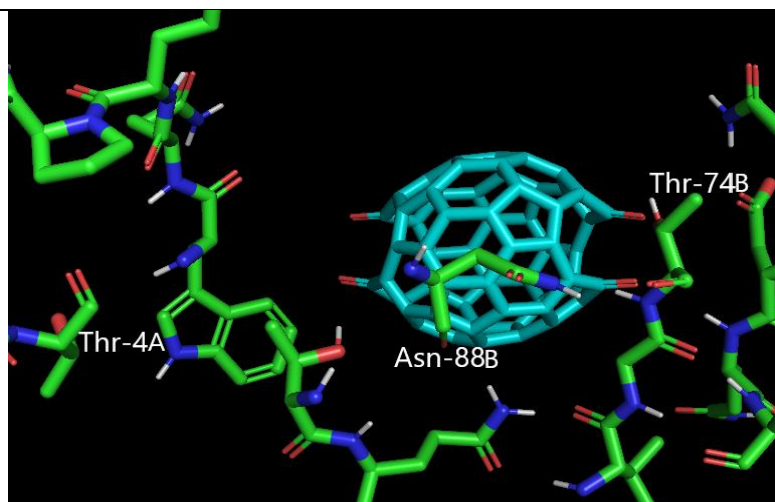


Figure 14i: C₆₀O₄-G conformation 9 with the HIV-PR (-8.7 kcal/mol)

C₆₀O₄-E

Table 5: C₆₀O₄-E Docking Results

Docking Poses	Affinity (kcal/mol)	H Bond Location	H Bond Distance (Å)	Comments
1	-9.5	O.1-Glu-92B O.2-Thr-74B O.3-Thr-74B O.3-Asn-88B O.4-Thr-74B	2.6, 2.4, 2.3, 1.9, 2.4	
2	-9.4	O.1-Thr-4A	1.7	
3	-9.4	O.1-Thr-74A O.2-Thr-74A O.2-Asn-88B O.3-Thr-74A	2.3, 2.4, 2.1, 2.3	
4	-9.2	O.2-Thr-74B O.3-Glu-7B	2.3, 2.6	
5	-9.2	O.2-Asn-88B O.3-Thr-74B O.4-Thr-74B	2.1, 2.1, 2.7	
6	-9.1	O.1-Glu-92B O.2-Glu-92B O.3-Asn-88A O.4-Thr-74A	2.3, 2.7, 2.3, 2.4	
7	-9	O.3-Thr-74A	2.2	
8	-9	O.1-Glu-92B O.3-Asn-88B O.4-Thr-74B	2.8, 2.3, 2.7	
9	-8.9	O.1-Thr-74B O.1-Asn-88B O.2-Thr-74B	2.1, 2.1, 2.2	

Table 5 details the binding affinity and H-bonds of each docking conformation for C₆₀O₄-E. C₆₀O₄-E has the carbonyl groups placed in a more localized region as each carbonyl creates an electropositive region beneath the electronegative oxygens. This results in a slightly less stable compound, but having more oxygens in one general location allows for more hydrogen bonding to the same residue(s) and consequently stronger binding affinity. Figure 15 shows the surface area view of HIV with the first docking pose, whereas figures 15a-I display the docking results for C₆₀O₄-E at Glu-7B, Glu-92B, Thr-4A, Asn-88B, Thr-74A, Thr-74B achieved through blind docking.

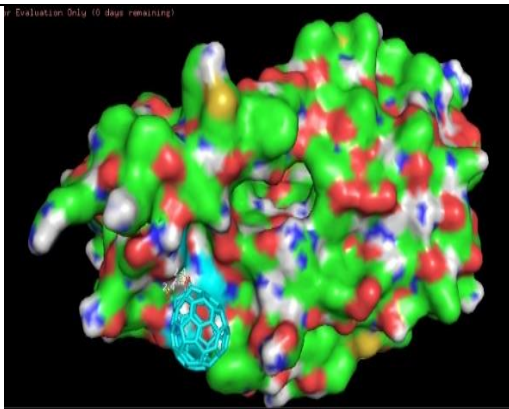


Figure 15: Surface area display of HIV-PR in PyMOL with pose C₆₀O₄-E 1

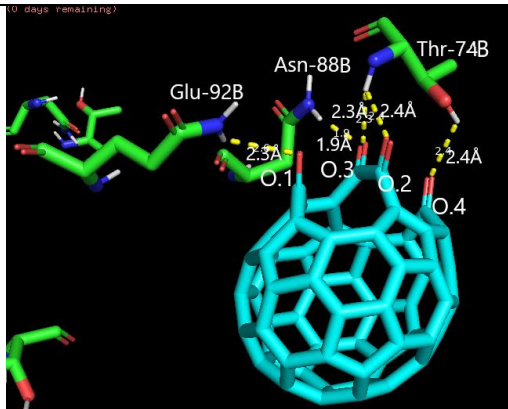


Figure 15a: C₆₀O₄-E conformation 1 with the HIV-PR (-9.5 kcal/mol)

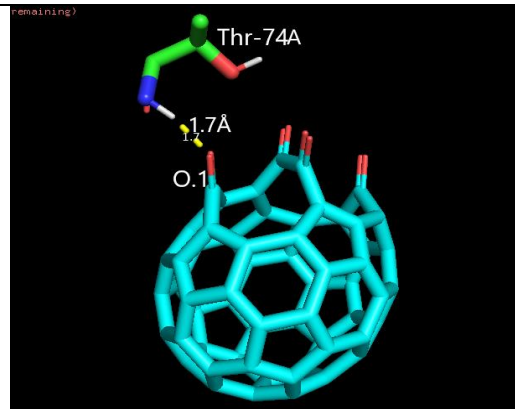


Figure 15b: C₆₀O₄-E conformation 2 with the HIV-PR (-9.4 kcal/mol)

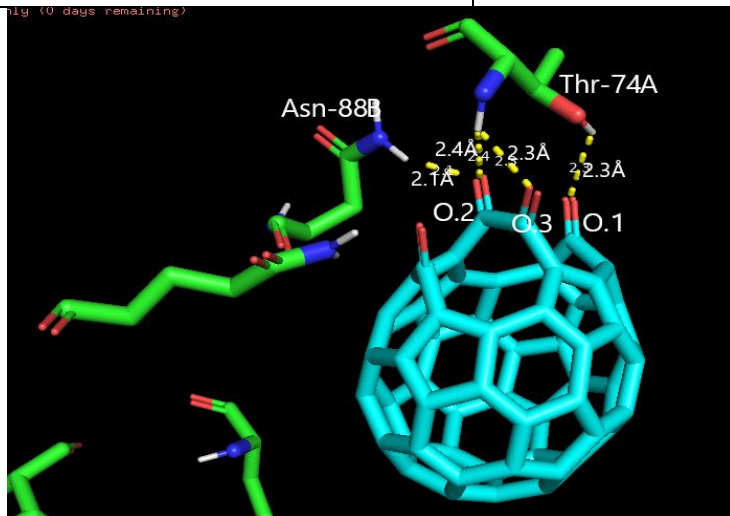


Figure 15c: C₆₀O₄-E conformation 3 with the HIV-PR (-9.4 kcal/mol)

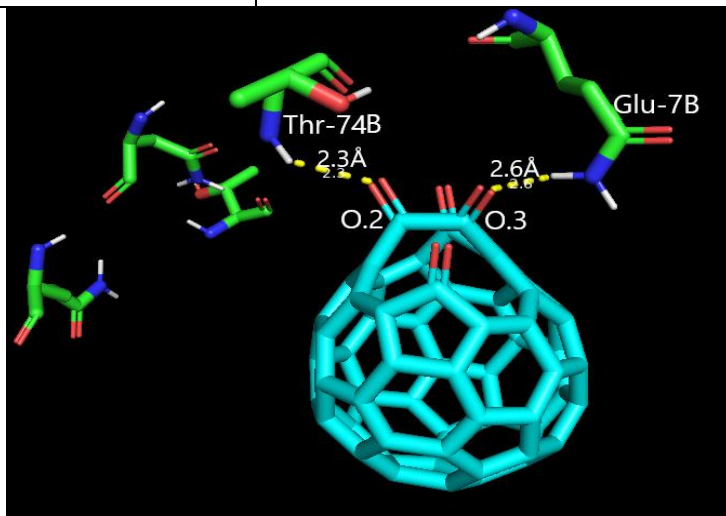


Figure 15d: C₆₀O₄-E conformation 4 with the HIV-PR (-9.2 kcal/mol)

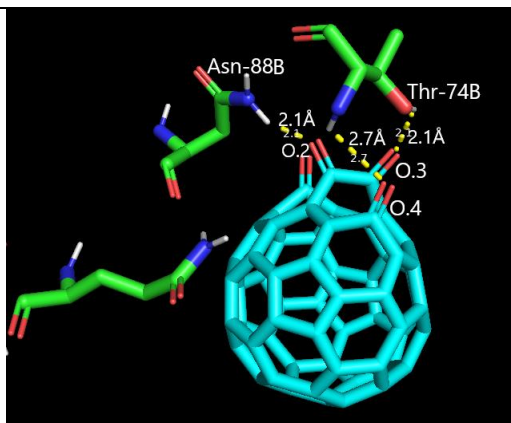


Figure 15e: C₆₀O₄-E conformation 5 with the HIV-PR (-9.2 kcal/mol)

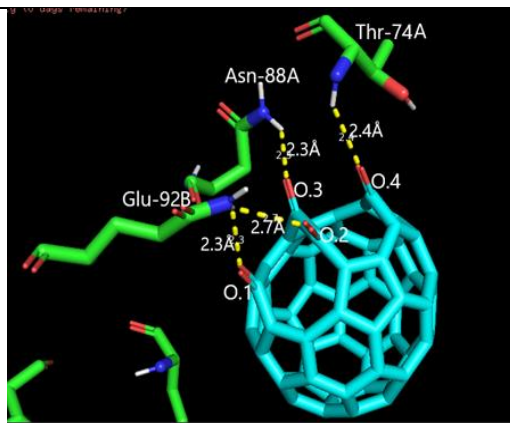


Figure 15f: C₆₀O₄-E conformation 6 with the HIV-PR (-9.1 kcal/mol)

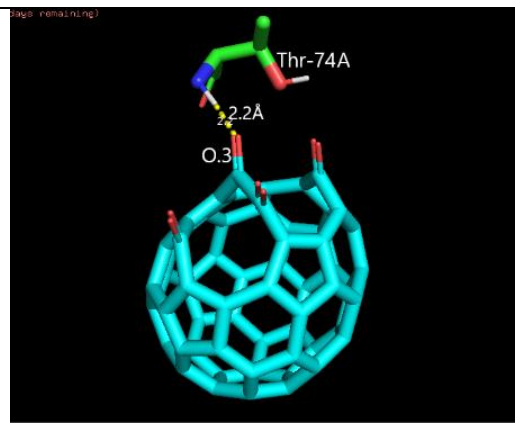


Figure 15g: C₆₀O₄-E conformation 7 with the HIV-PR (-9.0 kcal/mol)

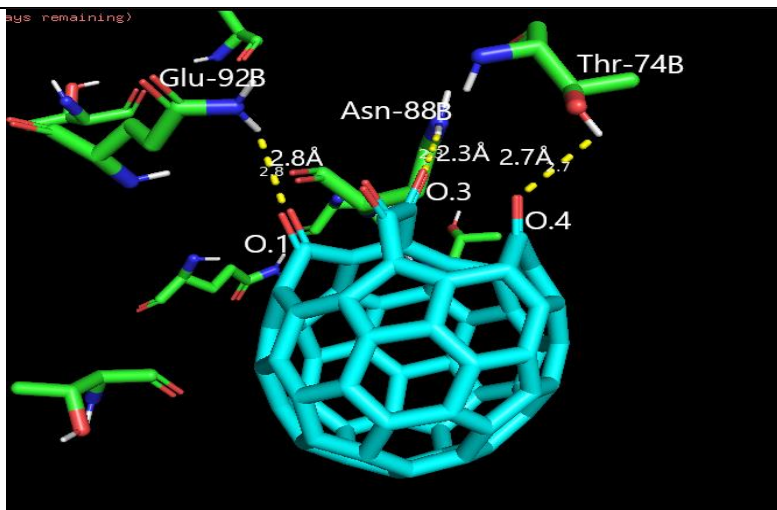


Figure 15h: C₆₀O₄-E conformation 8 with the HIV-PR (-9.0 kcal/mol)

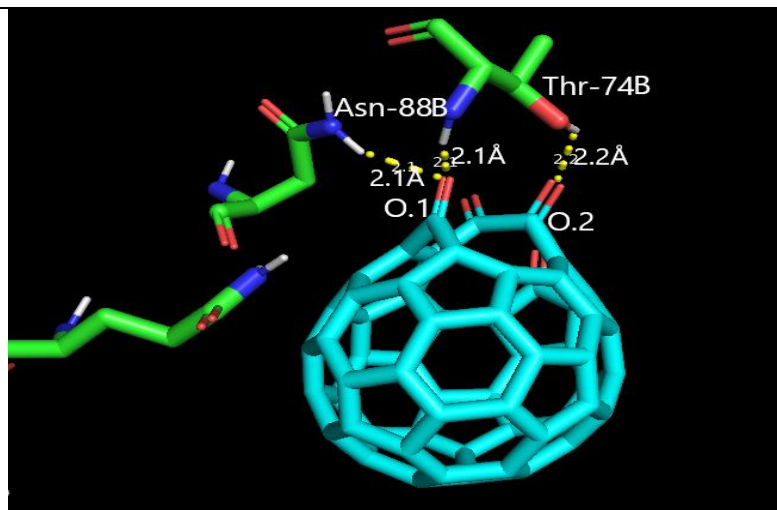


Figure 15i: C₆₀O₄-E conformation 9 with the HIV-PR (-8.9 kcal/mol)

C₆₀O₆-G

Table 6: C₆₀O₆-G Docking results

Docking Poses	Affinity (kcal/mol)	H Bond Location	H Bond Distance (Å)	Comments
1	-9.6	O.1-Thr-4A O.2-Thr-4A O.3-Leu-10A	2.5, 2.1, 2.5	O1 and O2 bonded to two different H atoms on Thr-4A
2	-9.4	O.1-Thr-4A	2.1	
3	-9.3	O.1-Thr-4A	1.9	
4	-9.3	O.1-Thr-74B O.2-Thr-74B O.2-Asn-88B	2.4, 2.2, 2.2	
5	-9.3	N/A		No H bond
6	-9.2	O.3-Leu-10A	2.5	
7	-9.2	O.3-Thr-91B O.4-Thr-91B	1.8, 2.5	
8	-9.1	O.2-Thr-4A	2.4	
9	-9.1	O.2-Thr-4A	2.1	

Table 6 details the binding affinity and H-bonds of each docking conformation for C₆₀O₆-G. Less hydrogen bonds are observed in this docking than with C₆₀O₄-E (24 compared to 13), but C₆₀O₆-G exhibits stronger binding affinity in its most stable conformation (-9.6 kcal/mol compared to -9.5 kcal/mol from C₆₀O₄-E). Poses 1, 2 3, 8, and 9 (Figures 16a, b, c, h, and i respectively) are alike in that they all exhibit H-bonds with Thr-4A. The docking results for C₆₀O₆-G at Thr-4A, Leu-10A, Thr-74B, Thr-91B and Asn-88B achieved through blind docking are displayed below in Figure 16, and Figures 16a-i.

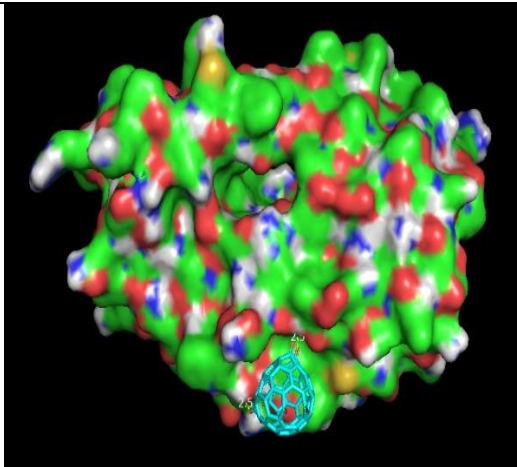


Figure 16: Surface area display of HIV-PR in PyMOL with pose C₆₀O₆-G 1

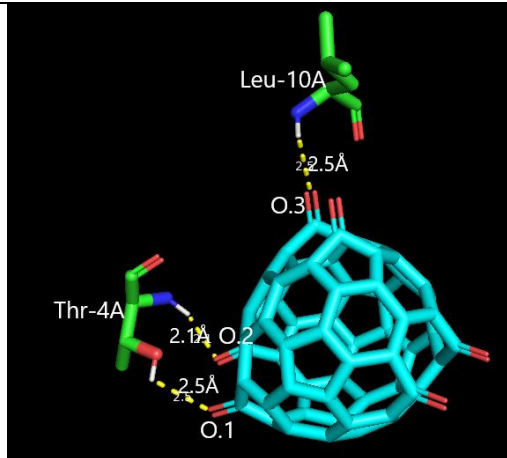


Figure 16a: C₆₀O₆-G conformation 1 with the HIV-PR
(-9.6 kcal/mol)

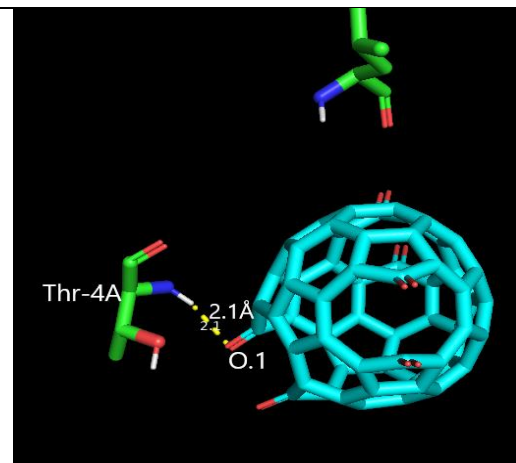


Figure 16b: C₆₀O₆-G conformation 2 with the HIV-PR
(-9.4 kcal/mol)

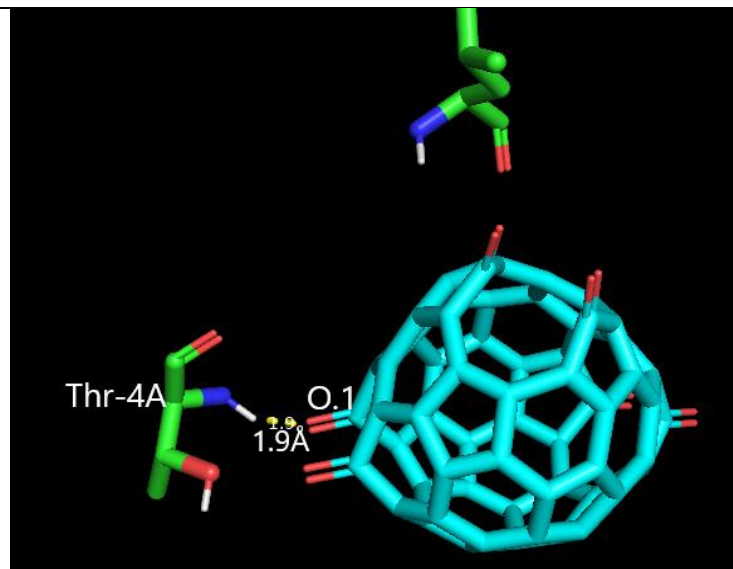


Figure 16c: C₆₀O₆-G conformation 3 with the HIV-PR
(-9.3 kcal/mol)

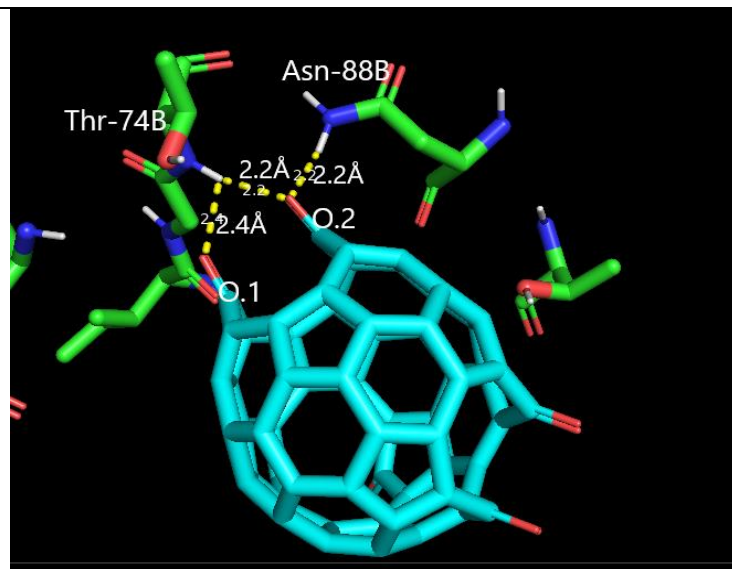


Figure 16d: C₆₀O₆-G conformation 4 with the HIV-PR
(-9.3 kcal/mol)

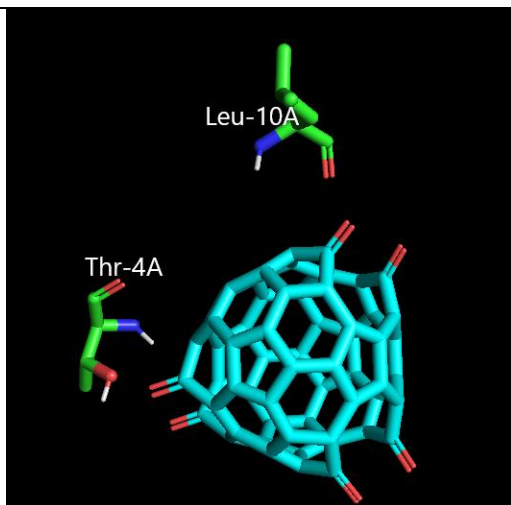


Figure 16e: C₆₀O₆-G conformation 5 with the HIV-PR (-9.3 kcal/mol)

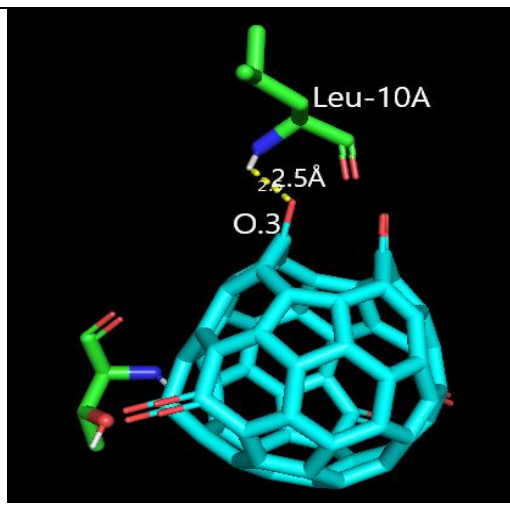


Figure 16f: C₆₀O₆-G conformation 6 with the HIV-PR (-9.2 kcal/mol)

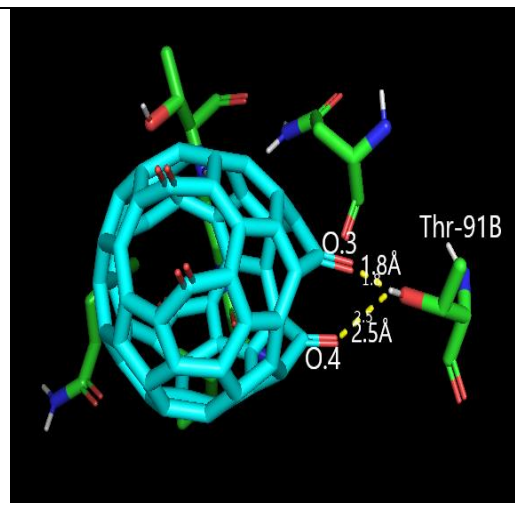


Figure 16g: C₆₀O₆-G conformation 7 with the HIV-PR (-9.2 kcal/mol)

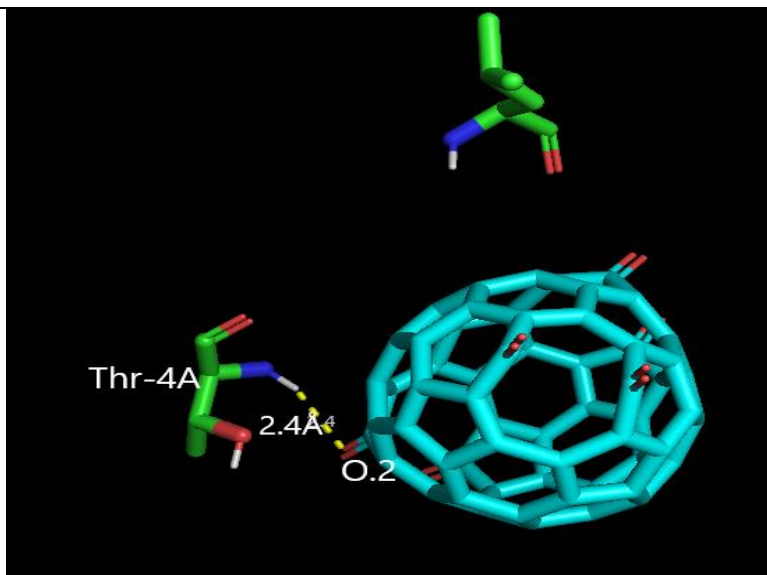


Figure 16h: C₆₀O₆-G conformation 8 with the HIV-PR (-9.1 kcal/mol)

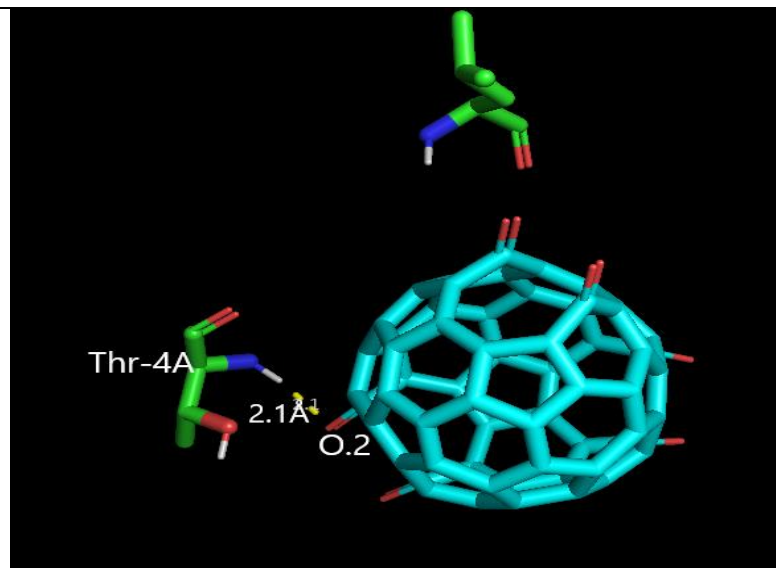


Figure 16i: C₆₀O₆-G conformation 9 with the HIV-PR (-9.1 kcal/mol)

C₆₀O₆-E

Table 7: C₆₀O₆-E Docking results

Docking Poses	Affinity (kcal/mol)	H Bond Location	H Bond Distance (Å)	Comments
1	-9.8	O.1-Thr-4A O.2-Thr-4A	2.5, 2.2	
2	-9.8	O.1-Thr-4A O.2-Thr-4A	2.6, 2.1	O.1 and O.2 bonded to two different H atoms on Thr-4A
3	-9.7	O.3-Asn-88B O.3-Thr-74B O.4-Thr-74B	2.2, 2.4, 2.2	O.3 and O.4 bonded to two different H atoms on Thr-74B
4	-9.6	O.1-Gln-92A O.3-Gln-92A O.4-Thr-74A O.5-Asn-88A O.6-Thr-74A	2.7, 2.2, 2.2, 2.3, 2.4	
5	-9.5	O.3-Thr-4B O.4-Gln-7B O.5-Leu-10B	2.6, 2.1, 2.8	
6	-9.3	O.1-Thr-74A O.2-Thr-74A	2.6, 2.3	O.1 and O.2 bonded to two different H atoms on Thr-74A
7	-9.3	O.1-Thr-74A O.2-Thr-74A O.3-Asn-88A	2.3, 2.2, 2.7	O.1 and O.2 bonded to two different H atoms on Thr-74A
8	-9.3	O.4-Thr-4A	2.0	
9	-9.2	O.4-Thr-4A	2.0	

Table 7 details the binding affinity and H-bonds of each docking conformation for C₆₀O₆-E. As seen between the two variants of C₆₀O₄, C₆₀O₆-E has a greater number of H-bonds than C₆₀O₆-G (22 compared to 13). A stronger binding affinity is seen in pose 1 (-9.8 kcal/mol) compared to pose 1 of C₆₀O₆-G (-9.6 kcal/mol). Below are the docking results for C₆₀O₆-E at Thr-4A, Thr-4B, Asn-88A, Asn-88B, Thr-74A, Thr-74B, Gln-92A, Thr-4B, Gln-7B, and Leu-10B achieved through blind docking displayed in Figures 17, and 17a-i.

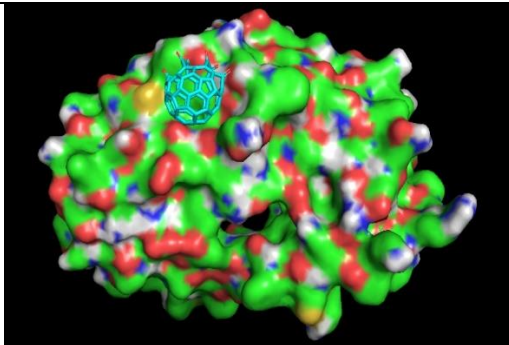


Figure 17: Surface area display of HIV-PR in PyMOL with pose C₆₀O₆-E 1

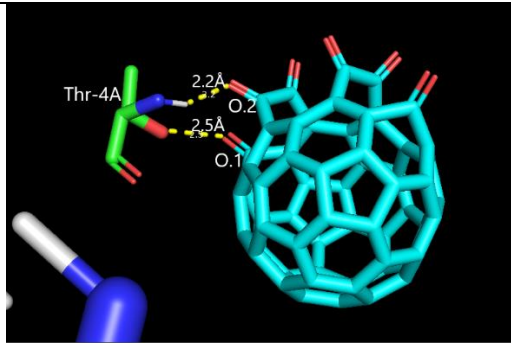


Figure 17a: C₆₀O₆-E conformation 1 with the HIV-PR (-9.8 kcal/mol)

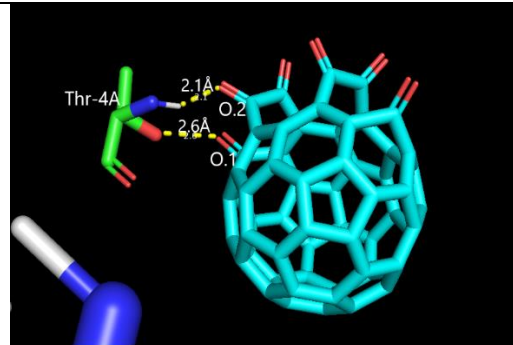


Figure 17b: C₆₀O₆-E conformation 2 with the HIV-PR (-9.8 kcal/mol)

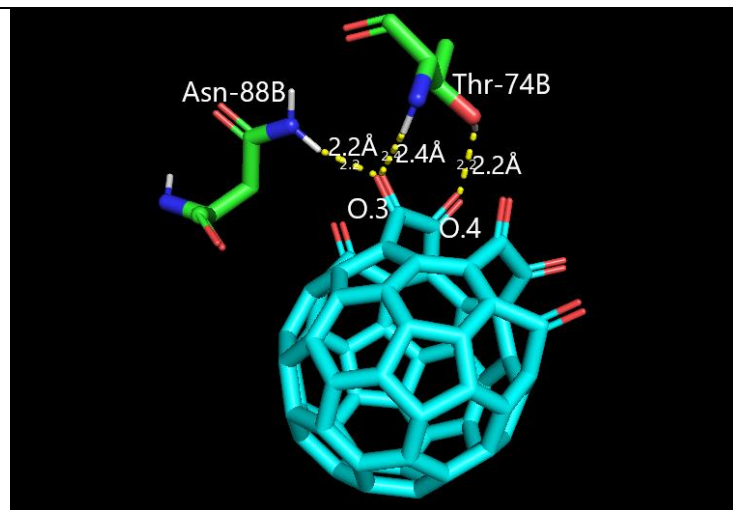


Figure 17c: C₆₀O₆-E conformation 3 with the HIV-PR (-9.7 kcal/mol)

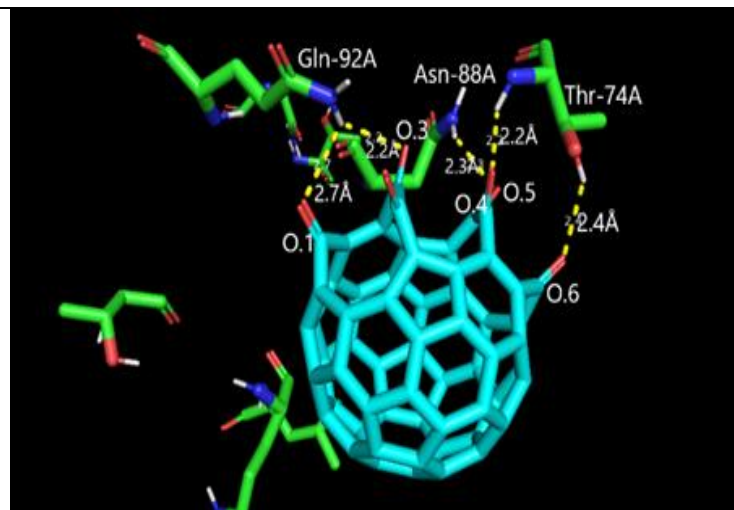


Figure 17d: C₆₀O₆-E conformation 4 with the HIV-PR (-9.6 kcal/mol)

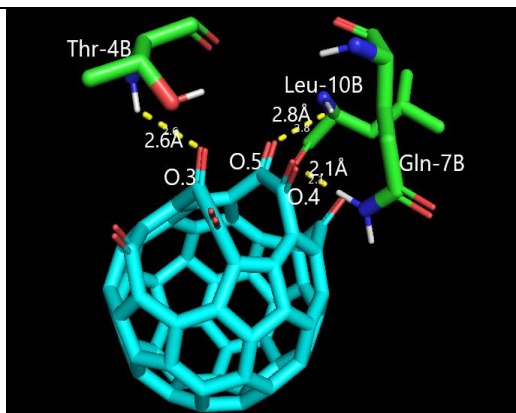


Figure 17e: C₆₀O₆-E conformation 5 with the HIV-PR (-9.5 kcal/mol)

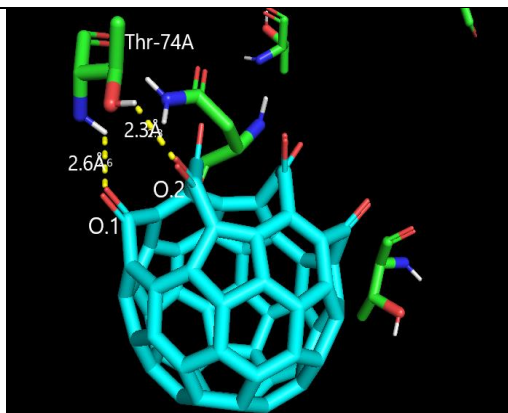


Figure 17f: C₆₀O₆-E conformation 6 with the HIV-PR (-9.3 kcal/mol)

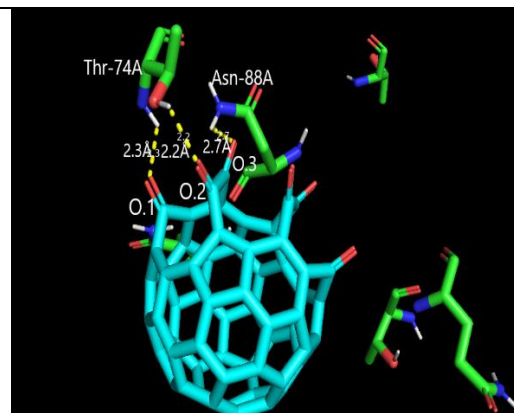


Figure 17g: C₆₀O₆-E conformation 7 with the HIV-PR (-9.3 kcal/mol)

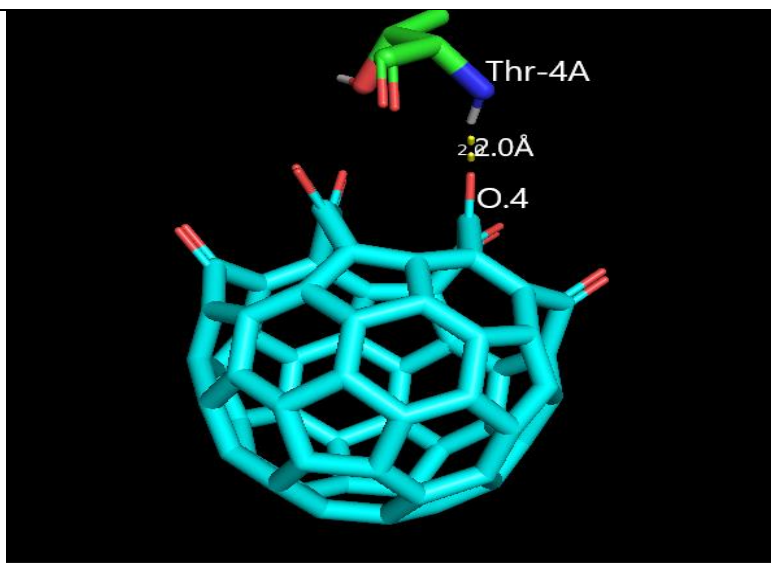


Figure 17h: C₆₀O₆-E conformation 8 with the HIV-PR (-9.3 kcal/mol)

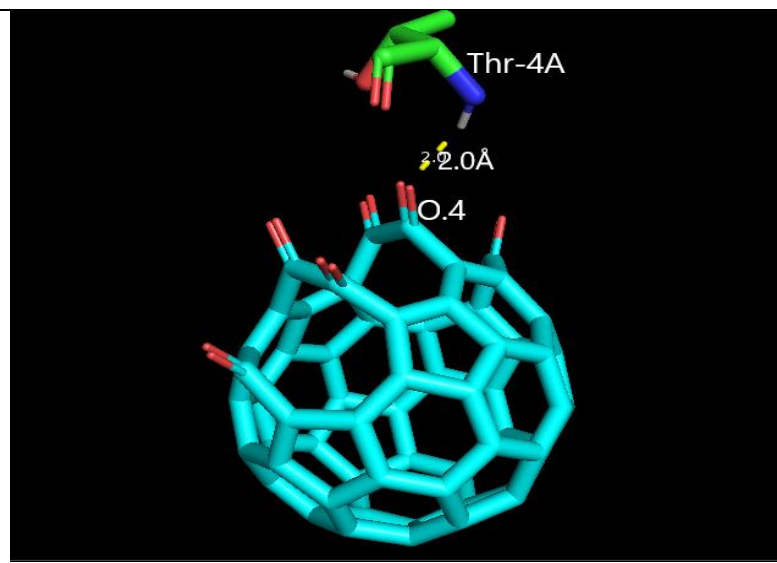


Figure 17i: C₆₀O₆-E conformation 9 with the HIV-PR (-9.2 kcal/mol)

C₆₀O₈-G

Table 8: C₆₀O₈-G Docking results

Docking Poses	Affinity (kcal/mol)	H Bond Location	H Bond Distance (Å)	Comments
1	-9.8	N/A		No H bond
2	-9.6	O.1-Gln-7B	2.4	
3	-9.4	O.1-Thr-91B O.2-Thr-91B	1.9, 2.5	
4	-9.4	O.1-Thr-4A	2	
5	-9.4	O.1-Gln-7A O.3-Arg-87B O.4-Arg-87B O.4-Arg-87B	2.3, 2.2, 2.2, 2.4	O.4 bonded to two different H atoms on Arg-87B
6	-9.4	O.1-Gln-7A O.2-Gln-7A O.3-Arg-87B O.4-Arg-87B O.4-Arg-87B	2.1, 2.6, 2.0, 2.2, 2.3	O.4 bonded to two different H atoms on Arg-87B
7	-9.3	N/A		No H bond
8	-9.3	O.1-Thr-4A	1.9	
9	-9.3	O.1-Thr-74B O.1-Asn-88B O.2-Thr-74B	1.8, 2.2, 2.5	

Table 8 details the binding affinity and H-bonds of each docking conformation for C₆₀O₈-G. The following docking run yielded a lower number of hydrogen bonds compared to C₆₀O₆-E (17 compared to 22) with an equal binding affinity between each structure's most stable pose (-9.8 kcal/mol). Interestingly, the most stable pose in this set had no H-bonds, indicating strong dipole and van der waals interactions between neighboring residues are present. Pose 6 (Figure 18f) has the highest number of H-bonds out of any conformation in the entire experiment. Below are the docking results for C₆₀O₈-G at Gln-7A, Gln-7B, Thr-91B, Thr-4A, Arg-87B, Thr-74B, and Asn-88B achieved through blind docking displayed in Figures 18, and 18a-i.

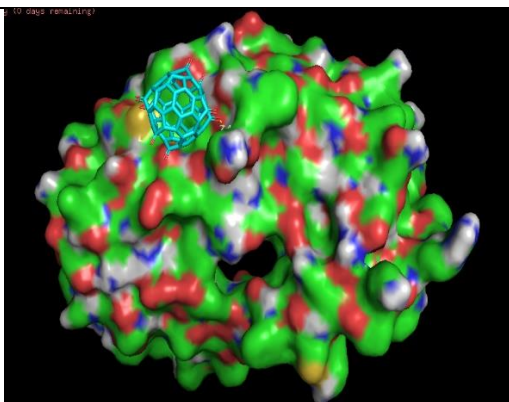


Figure 18: Surface area display of HIV-PR in PyMOL with pose C₆₀O₈-G 1

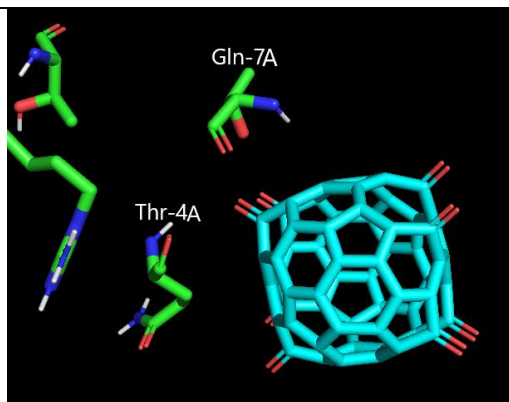


Figure 18a: C₆₀O₈-G conformation 1 with the HIV-PR (-9.8 kcal/mol)

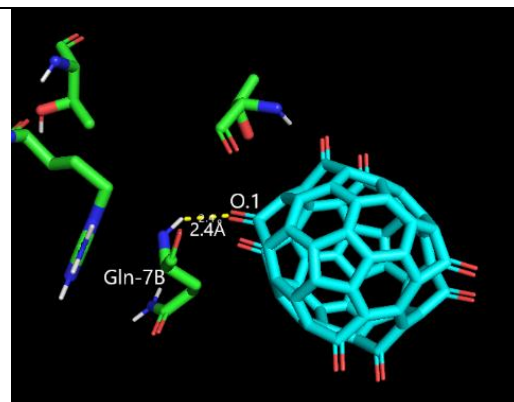


Figure 18b: C₆₀O₈-G conformation 2 with the HIV-PR (-9.6 kcal/mol)

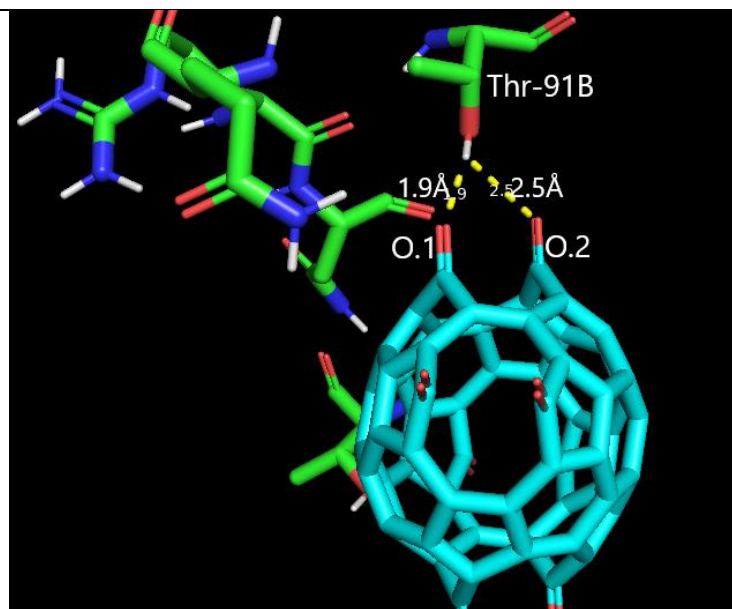


Figure 18c: C₆₀O₈-G conformation 3 with the HIV-PR (-9.4 kcal/mol)

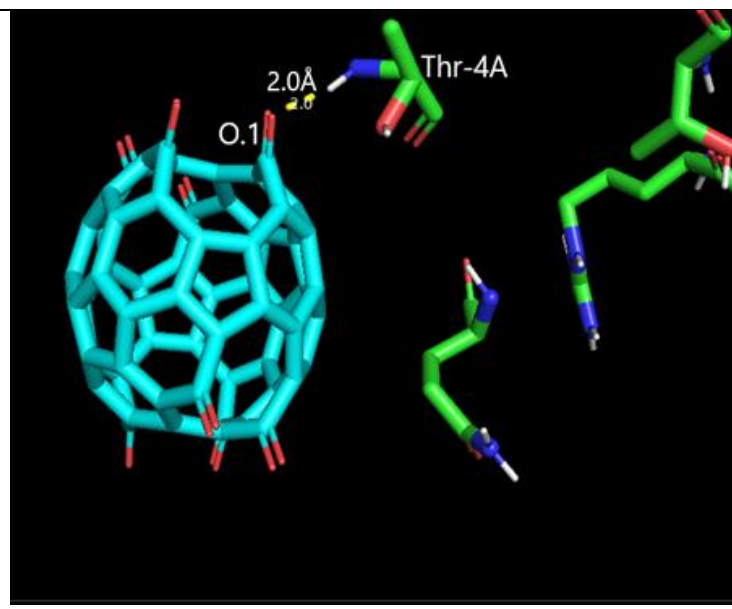


Figure 18d: C₆₀O₈-G conformation 4 with the HIV-PR (-9.4 kcal/mol)

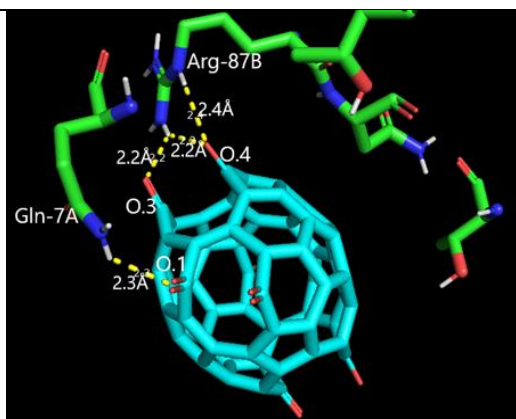


Figure 18e: C₆₀O₈-G conformation 5 with the HIV-PR (-9.4 kcal/mol)

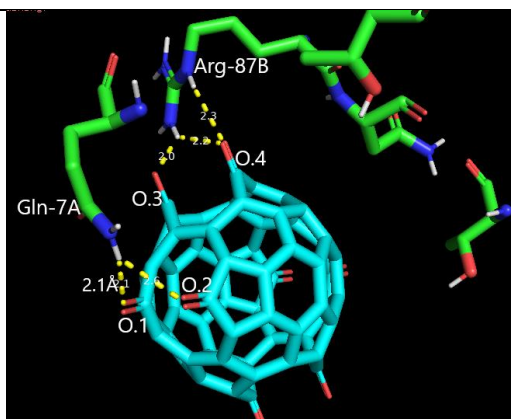


Figure 18f: C₆₀O₈-G conformation 6 with the HIV-PR (-9.4 kcal/mol)

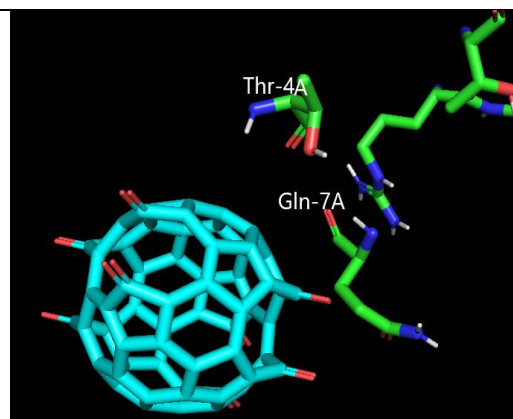


Figure 18g: C₆₀O₈-G conformation 7 with the HIV-PR (-9.3 kcal/mol)

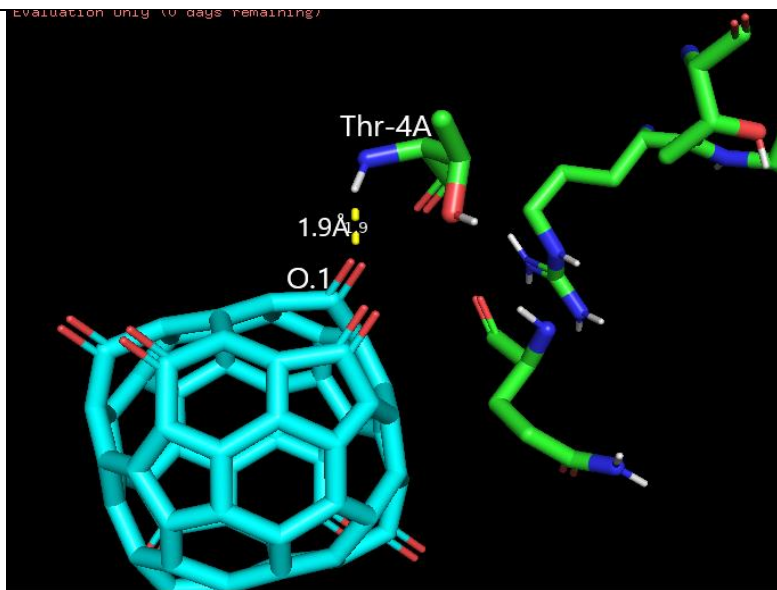


Figure 18h: C₆₀O₈-G conformation 8 with the HIV-PR (-9.3 kcal/mol)

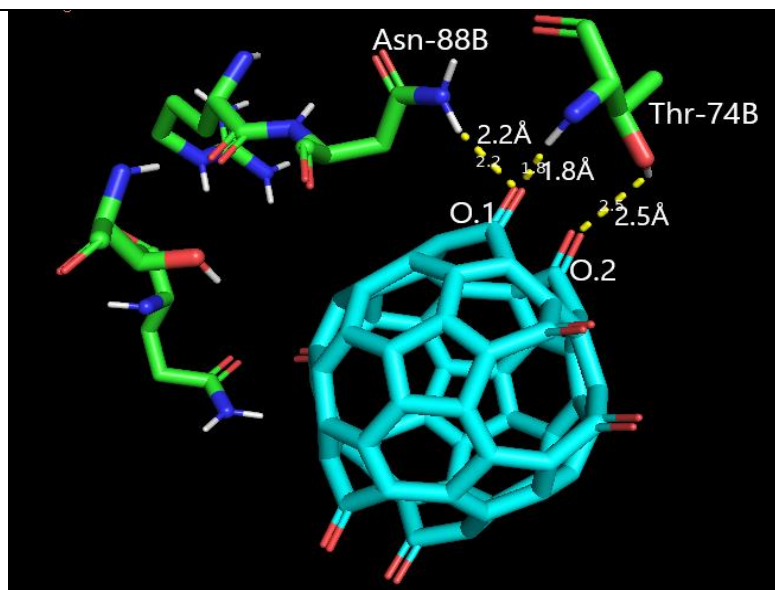


Figure 18i: C₆₀O₈-G conformation 9 with the HIV-PR (-9.3 kcal/mol)

C₆₀O₈-E**Table 9:** C₆₀O₈-E Docking results

Docking Poses	Affinity (kcal/mol)	H Bond Location	H Bond Distance (Å)	Comments
1	-10.4	O.2-Thr-74B O.5-Thr-74B O.6-Asn-88B	2.2, 2.4, 2.2	O.2 and O.3 bonded to two different H atoms on Thr-74B
2	-10.2	O.6-Asn-88B O.6-Thr-74B O.8-Thr-74B	2.2, 2.5, 2.2	
3	-10.1	O.1-Gln-92A O.2-Gln-92A O.4-Thr-74A O.5-Thr-74A	2.6, 2.3, 2.1, 2.6	O.4 and O.5 bonded to two different H atoms on Thr-74B
4	-10	O.4-Thr-74B O.4-Asn-88B O.8-Thr-74B	1.9, 2.4, 2.5	
5	-10	O.1-Thr-74B O.2-Asn-88B O.3-Thr-74B	2.7, 2.2, 2.3	O.1 and O.3 bonded to two different H atoms on Thr-74B
6	-9.9	O.4-Asn-88A O.4-Thr-74A O.5-Thr-74A O.8-Thr-74A	2.4, 2.0, 2.7, 2.5	O.8 bonded to a different H atom on Thr-74A than O.4 and O.5
7	-9.9	O.7-Thr-4A	2.4	
8	-9.7	O.2-Gln-92B O.2-Asn-88B O.4-Thr-74B O.5-Thr-74B	2.8, 2.6, 2.4, 2.0	O.4 and O.5 bonded to two different H atoms on Thr-74B
9	-9.5	N/A		

Table 9 details the binding affinity and H-bonds of each docking conformation for C₆₀O₈-E. The results for this docking run exhibit the same patterns as observed previously, more hydrogen bonds (25 compared to 17 in C₆₀O₈-G) and stronger binding (-10.4 kcal/mol compared to -9.8 kcal/mol from C₆₀O₈-G). Below are the docking results for C₆₀O₈-E at Thr-74B, Asn-88B, Gln-92A, Thr-74A, Asn-88A, Thr-4A achieved through blind docking. Surface area view is shown in Figure 19, and the docking results are shown in Figures 19a-i.

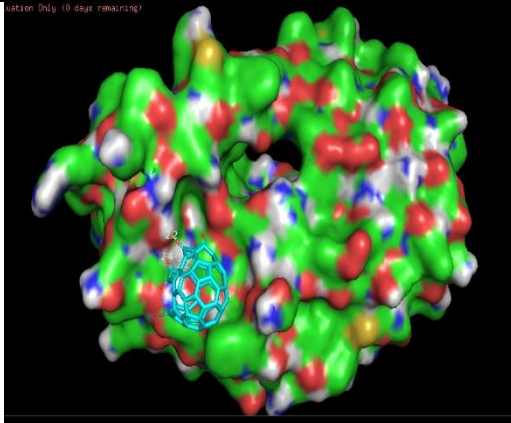


Figure 19: Surface area display of HIV-PR in PyMOL with pose C₆₀O₈-E 1

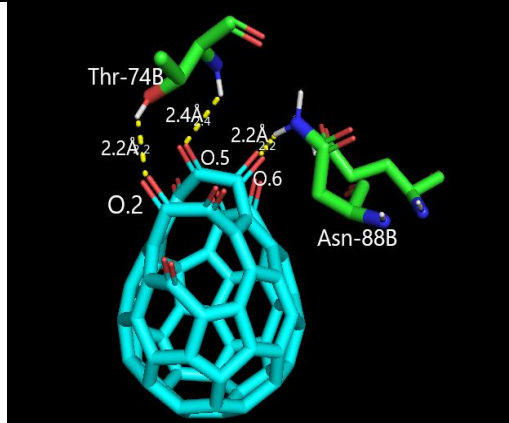


Figure 19a: C₆₀O₈-E conformation 1 with the HIV-PR (-10.4 kcal/mol)

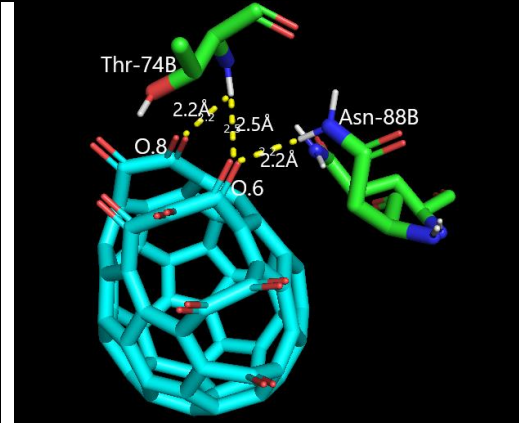


Figure 19b: C₆₀O8-E conformation 2 with the HIV-PR (-10.2 kcal/mol)

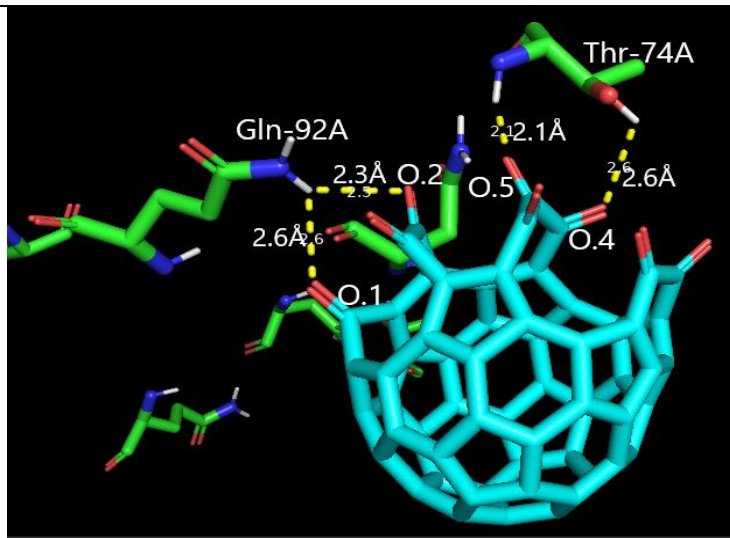


Figure 19c: C₆₀O₈-E conformation 3 with the HIV-PR (-10.1 kcal/mol)

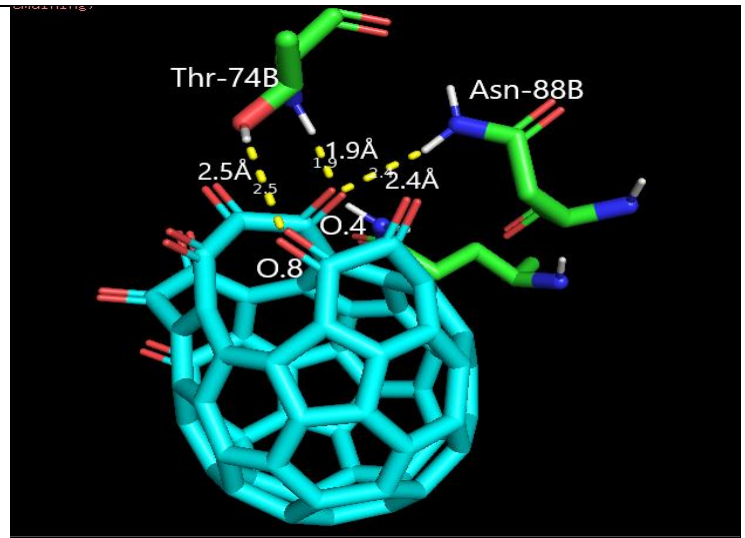


Figure 19d: C₆₀O₈-E conformation 4 with the HIV-PR (-10.0 kcal/mol)

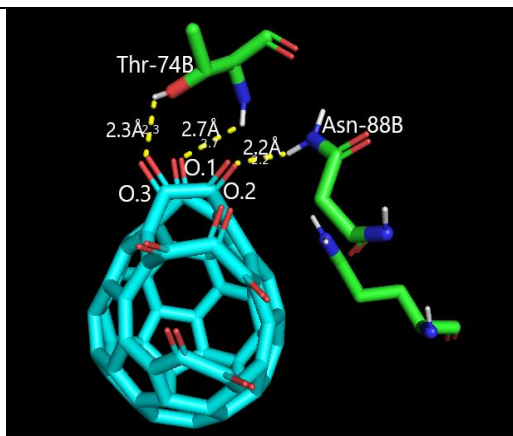


Figure 19e: C₆₀O₈-E conformation 5 with the HIV-PR (-10.0 kcal/mol)

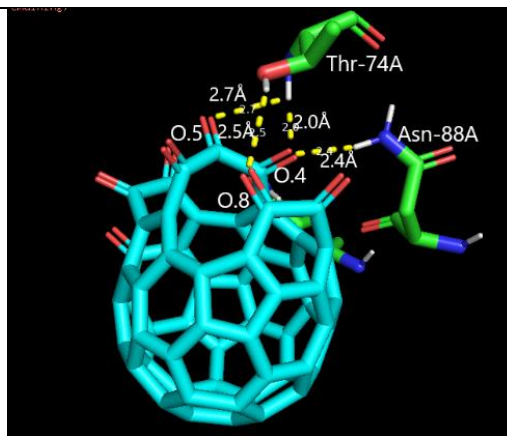


Figure 19f: C₆₀O₈-E conformation 6 with the HIV-PR (-9.9 kcal/mol)

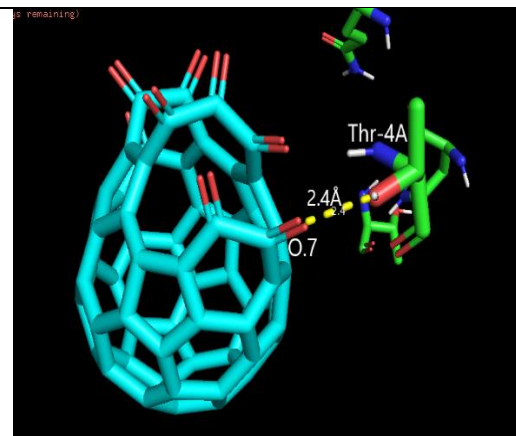


Figure 19g: C₆₀O₈-E conformation 7 with the HIV-PR (-9.9 kcal/mol)

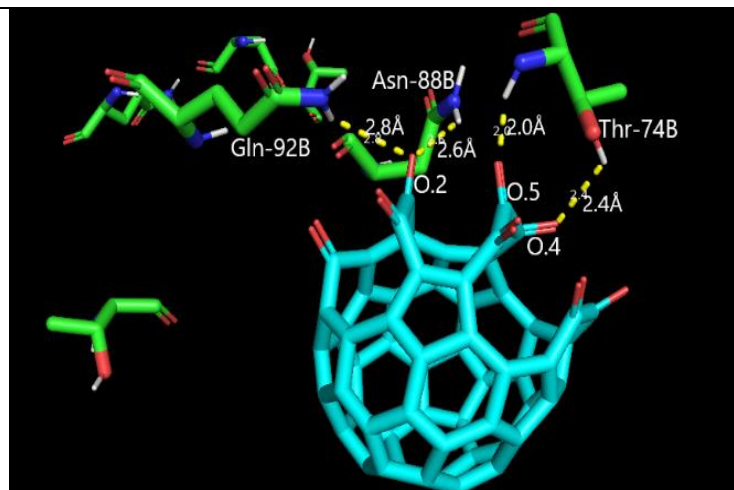


Figure 19h: C₆₀O₈-E conformation 8 with the HIV-PR (-9.7 kcal/mol)

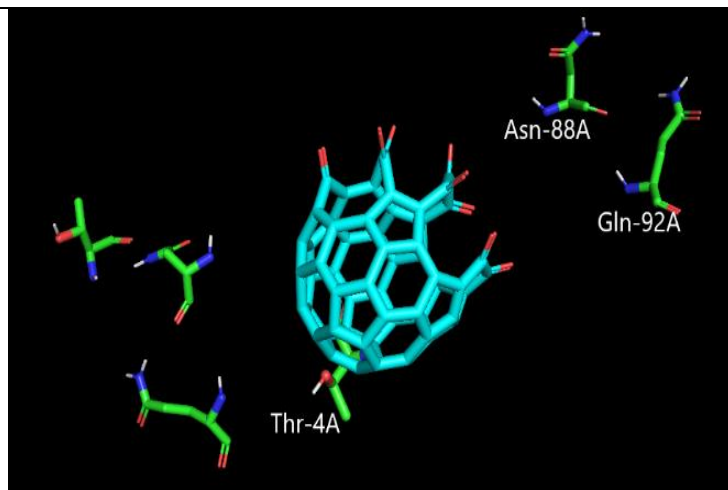


Figure 19i: C₆₀O₈-E conformation 9 with the HIV-PR (-9.5 kcal/mol)

Discussion:

The blind docking simulations yielded high stability docking conformations (binding affinities $-10.4 \leq -8.1$ kcal/mol). Generally, more oxygens in a fullerene structure yielded a greater number of hydrogen bonds and a higher binding affinity in docking. Between the geometrical and electrostatic variants of each fullerene structure, the latter displayed higher binding affinity in its conformations. The electrostatic structures can form more H bonds to the same localized residues, resulting in more stable conformations. Dipole-dipole and van der Waals interactions were found to have played a significant role in binding as many conformations exhibited strong binding (≥ -9.8 kcal/mol) with 0 hydrogen bonds. The electrostatic variants of structures had a higher chemical energy of $\bar{x} = 4447.44$ KJ/mol ($\bar{x} = 4192.39$ KJ/mol for the geometric structures according to Spartan) making these structures less stable and therefore less probable to form during synthesis. It is posited that the ability to inhibit the HIV-PR observed in Kumar's study is largely due to the strong binding affinity $C_{60}O_x$ fullerenes have to the HIV-PR. In Chang et al.'s report on the first phase of FightAIDS@Home, binding affinities ≤ -7.0 kcal/mol were considered effective for inhibiting HIV-PR replication.¹³ Following this, it is easy to see how these fullerene structures were able to act as effective inhibitors in Kumar's work with a minimum of -8.1 kcal/mol.

The use of blind docking did not cause issues for experiment run time as AutoDock Vina was effectively able to utilize all twenty cores in the CPU used for the experiment. At a glance, the blind dockings between different structures appear vastly inconsistent in terms of the residues bonded to. However, counting the number of times each residue experienced hydrogen bonding displays a generalized preference to certain binding sites across all $C_{60}O_x$ structures. Figure 20 below provides a visualization of the number of times each amino acid residue in the HIV-PR experienced hydrogen bonding from $C_{60}O_x$ ligands across all docking simulations:

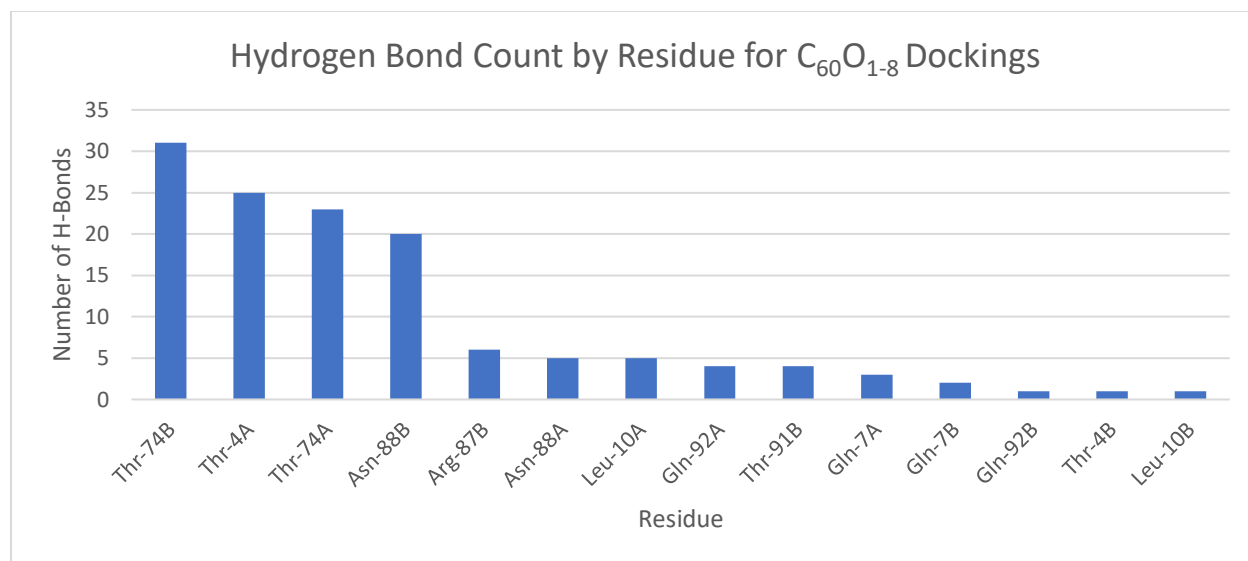


Figure 20: Hydrogen bonded residues in docking studies

Figure 20 shows a strong preference across all conformations for a select few residues, particularly Thr-74B, Thr-4A, Thr-74A and Asn-88B. These residues are near the Asp-29A, Asp-29B active site for this HIV-PR structure. This implies a preference for oxygenated fullerenes to bind to the general active site region of the HIV-PR in blind docking simulations even under default docking parameters. Unlike other ligand inhibitors, the larger size of C₆₀ (1.1nm or 11Å) makes it more difficult to fit directly into the open space where the Asp-29A and Asp-29B active site residues reside²⁵. These docking simulations suggest that oxygenated fullerene structures do not inhibit the reproduction of the HIV-PR by directly binding to the active sites during replication, but rather via allosteric inhibition causing an upset in the conformation equilibrium of the HIV-PR that prevents it from carrying out its proper function. Figure 21 presents the stick form of the HIV-PR in PyMOL with the active site Asp-29A and Asp-29B residues depicted in red and Thr-74B, Thr-4A, Asn-88B and Thr-74A depicted in cyan. The red boxes are enclosed around the active site residues whereas the blue circles are around the residues where hydrogen bonding was commonly observed to the latter residues with C₆₀O_x.

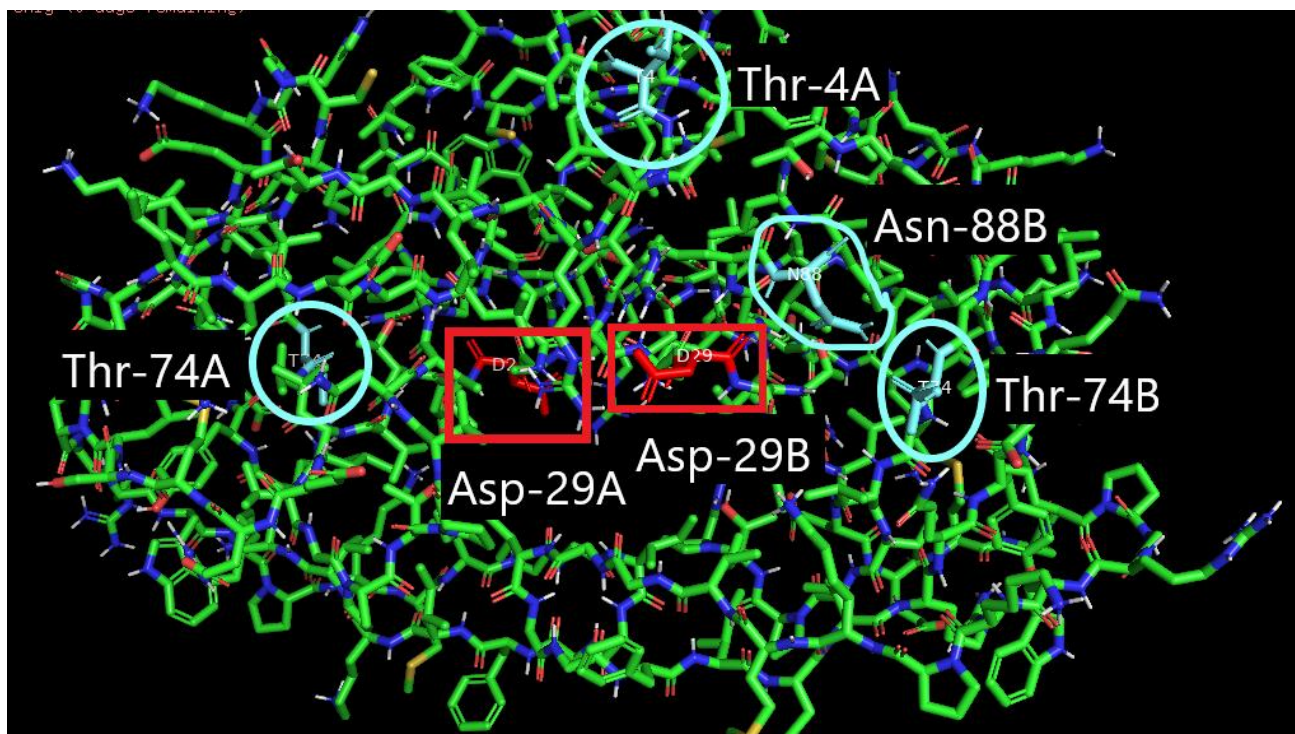


Figure 21: HIV-PR in PyMOL comparing active site and common binding sites in the docking study

Future work would focus on improving reproducibility of blind docking experiments, investigation of more fullerene structures, and the use of more software. An alternate variant of AutoDock Vina titled “QuickVina,” produced by Amr Alhossary and Nafisa Mohamed, was found to have higher accuracy/reproducibility for blind docking experiments.²⁶ Exhaustiveness levels within the configuration files for docking runs should be increased to augment accuracy beyond default parameters. Structures like $C_{60}O_3$, $C_{60}O_5$, $C_{60}O_7$, $C_{60}O_{10}$, and $C_{60}O_{12}$ could be experimented with as well as more than two variants per structure. More probable isomers of these structures can be experimented with as well (structures like $C_{60}O_6$ -E and $C_{60}O_8$ -E are less likely to appear as depicted due to poor stability from electron repulsion due to close placement of the oxygens). More trials run of each experiment would improve quality control and validation of data gathered.

Conclusion:

Kumar's experiment on oxygenated fullerenes found that oxygenated buckminsterfullerene (C_{60}) structures produced via ozonolysis displayed IC_{50} at 1mg/mol^6 . Models of the oxygenated buckminsterfullerene compounds ($C_{60}O_x$) were created in Spartan software and docked to an HIV-PR crystal structure from The Brookhaven Protein Data Bank. Blind docking simulations were performed using AutoDock Vina under default parameters and analyzed in PyMOL software. The scoring function from AutoDock Vina depicts a strong binding affinity (≤ -8.1 kcal/mol) for all $C_{60}O_x$ variants. The strong binding affinity is posited to be a major factor in $C_{60}O_x$'s ability to inhibit HIV-PR replication. Several hydrogen bonds were observed and measured using PyMOL for all $C_{60}O_x$ structures. Analysis in PyMOL depicted a strong preference for hydrogen bonding to residues close but not at the active site of the HIV-PR (Asp-29), implying that the oxygenated fullerenes disrupt the HIV-PR through allosteric inhibition. These hydrogen bonds are theorized to play a key role in the $C_{60}O_x$'s binding affinity and HIV-PR inhibition. An effective antiretroviral drug will inhibit viral replication at low concentration with low cytotoxicity and high bioavailability. Docking studies will continue to play a vital role in discovering the characteristics of compounds at the molecular level that result in these desired properties.

References

- ¹ Roser, M. Ritchie, H. HIV / AIDS, *Our World In Data*, November 2019, <https://ourworldindata.org/hiv-aids#how-have-deaths-from-hiv-aids-changed-over-time>, (Accessed 2023-06-16)
- ² Kemnic, T.R.; Gulick, P.G. *HIV Antiretroviral Therapy*. National Library of Medicine (NIH), StatPearls Publishing, 2023
- ³ Carter, A.; Williams, A. HIV Treatments: List of Prescription Medications, *Healthline*, July 28, 2022, <https://www.healthline.com/health/hiv-aids/medications-list>, (Accessed 2023-06-16)
- ⁴ Aoki, M.; Hayashi, H.; Yedidi, R.; Martyr, C.; Takamatsu, Y.; Aoki-Ogata, H.; Nakamura, T.; Nakata, H.; Das, D.; Yamagata, Y.; Ghosh, A.; Mitsuya, H. The C5-substituted Tetrahydropyrano-tetrahydrofuran-derived Protease Inhibitors (PIs) Exert Potent Inhibition of the Replication of HIV-1 Variants Highly Resistant to Various PIs Including Darunavir. *Journal of Virology*. 2015, 90(5), 2180-2194. DOI: [10.1128/JVI.01829-15](https://doi.org/10.1128/JVI.01829-15)
- ⁵ World Health Organization, *Global action plan on HIV drug resistance 2017-2021: 2018 progress report, July 2018: Executive Summary*, World Health Organization, 2018, <https://www.who.int/publications/i/item/WHO-CDS-HIV-18.12>, (Accessed 2023-06-18)
- ⁶ Kumar, S.; Malhotra, R.; Satyam, A. Ozonolysis of [60] Fullerene. *Journal of the Chemical Society, Chemical Communications*, 1994, 11
- ⁷ Kumar, S.; Malhotra, R.; Satyam, A.; Narang, S.C.; Tse, D.S.; Ruoff, R.S.; Lorents, D.C. Approaches to chemical functionalization of fullerenes, *Transactions of the Material Research Society of Japan*, 1994, 14B
- ⁸ Trott, O.; Olson, A.J. *What is AutoDock?*, <https://autodock.scripps.edu/>, (Accessed 2023-06-25)
- ⁹ Berman, H.M.; Westbrook, J.; Feng, Z.; Gilliland, G.; Bhat, T.N.; Weissig, H.; Shindyalov, I.N.; Bourne, P.E. The Protein Data Bank. *Nucleic Acids Research*, 2000, 28(1), 235-242. DOI: [10.1093/nar/28.1.235](https://doi.org/10.1093/nar/28.1.235)
- ¹⁰ Trott, O.; Olson, A.J., AutoDock Vina: Improving The Speed and Accuracy of Docking With a New Scoring Function, Efficient Optimization and Multithreading. *Journal of Computational Chemistry*, 2010, 31(2), 455–461. DOI: [10.1002/jcc.21334](https://doi.org/10.1002/jcc.21334)
- ¹¹ Chang, M.W.; Ayeni, C.; Breuer, S.; Torbett, B.E. Virtual Screening for HIV Protease Inhibitors: A Comparison of AutoDock 4 and Vina. *PLOS ONE*, 2010, 5(8), 11955. DOI: [10.1371/journal.pone.0011955](https://doi.org/10.1371/journal.pone.0011955)
- ¹² Su, M.; Yang, Q.; Du, Y.; Feng, G.; Liu, Z.; Li, Y.; Wang, R. Comparative Assessment of Scoring Functions: The CASF-2016 Update. *Journal of Chemical Information and Modeling*, 2018, 59(2), 895-913.
- ¹³ Razzaghi-Asl, N.; Sepehri, S.; Ebadi, A.; Miri, R.; Shahabipour, S. Effect of Biomolecular Conformation on Docking Simulation: A Case Study on a Potent HIV-1 Protease Inhibitor. *Iranian journal of pharmaceutical research*, 2014, 14(3), 785-802

- ¹⁴ Chang, M.W.; Lindstrom, W.; Olson, A.J.; Belew, R.K. Analysis of HIV Wild-Type and Mutant Structures via in Silico Docking against Diverse Ligand Libraries. *Journal of Chemical Information and Modeling*, 2007, 47(3), 1258-1262. DOI: [10.1021/ci700044s](https://doi.org/10.1021/ci700044s)
- ¹⁵ Temesgen, Z.; Warnke, D.; Kasten, M.J. Current status of antiretroviral therapy. *Expert Opin Pharmacother*, 2006, 7(12), 1541-1554. DOI: [10.1517/14656566.7.12.1541](https://doi.org/10.1517/14656566.7.12.1541)
- ¹⁶ Perryman, A.L.; Santiago, D.N.; Forli, S.; Martins, D.S.; Olson, A.J. Virtual screening with AutoDock Vina and the common pharmacophore engine of a low diversity library of fragments and hits against the three allosteric sites of HIV integrase: participation in the SAMPL4 protein-ligand binding challenge, *Journal of computer-aided molecular design*, 2014, 28(4), 429–441. DOI: [10.1007/s10822-014-9709-3](https://doi.org/10.1007/s10822-014-9709-3)
- ¹⁷ Schinazi, R.; Sijbesma, R.P.; Srdanov, G.; Hill, C.; Wudl, F. Synthesis and virucidal activity of a water-soluble, configurationally stable, derivatized C60 fullerene, *Antimicrobial Agents and Chemotherapy*, 1993, 37(8), 1707-1710. DOI: [10.1128/AAC.37.8.1707](https://doi.org/10.1128/AAC.37.8.1707)
- ¹⁸ Bosi, S.; Da Ros, T.; Spalluto, G.; Balzarini, J.; Prato, M. Synthesis and Anti-HIV Properties of new water-soluble bis-functionalized[60]fullerene derivatives, *Bioorganic & Medicinal Chemistry Letters*, 2003, 13(24), 4437-4440. DOI: [10.1016/j.bmcl.2003.09.016](https://doi.org/10.1016/j.bmcl.2003.09.016)
- ¹⁹ Hassan, N.M.; Alhossary, A.A.; Muh, Y.; Kwoh, C.K. Protein-Ligand Blind Docking Using QuickVina-W With Inter-Process Spatio-Temporal Integration. *Scientific Reports*, 2017, 7, 15451. DOI: [10.1038/s41598-017-15571-7](https://doi.org/10.1038/s41598-017-15571-7)
- ²⁰ Wong, S.; Lightstone, F. Accounting for water molecules in drug design: A Review. *Expert Opinion On Drug Discovery*, 2011, 6(1), 65-74. DOI: [10.1517/17460441.2011.534452](https://doi.org/10.1517/17460441.2011.534452)
- ²¹ Lemmon, G.; Meiler, J. Towards ligand docking including explicit interface water molecules. *PLOS ONE*, 2013, 8(6). DOI: [10.1371/journal.pone.0067536](https://doi.org/10.1371/journal.pone.0067536)
- ²² Terefe, E.M.; Ghosh, A. Molecular Docking, Validation, Dynamics Simulations, and Pharmacokinetic Prediction of Phytochemicals Isolated From *Croton dichogamus* Against the HIV-1 Reverse Transcriptase. *Bioinformatics and Biology Insights*. 2022, 16. DOI: [10.1177/11779322221125605](https://doi.org/10.1177/11779322221125605)
- ²³ Cho, A.E.; Guallar, V.; Berne, B.J.; Friesner, R. Importance of accurate charges in molecular docking: quantum mechanical/molecular mechanical (QM/MM) approach. *Journal of Computational Chemistry*. 2005, 26(9), 915-931. DOI: [10.1002/jcc.20222](https://doi.org/10.1002/jcc.20222)
- ²⁴ Agarwal, R.C.; Smith, J.C. Speed vs Accuracy: Effect on Ligand Pose Accuracy of Varying Box Size and Exhaustiveness in AutoDock Vina. *Molecular Informatics*, 2022, 42(2). DOI: [10.1002/minf.202200188](https://doi.org/10.1002/minf.202200188)
- ²⁵ Qiao, R.; Roberts, A. P.; Mount, A. S.; Klaine, S. J.; Ke, P. C. Translocation of C₆₀ and its derivatives across a lipid bilayer. *Nano letters*. 2007, 7(3), 614–619. DOI: [10.1021/nl062515f](https://doi.org/10.1021/nl062515f)
- ²⁶ Alhossary, A.; Handoko, S.D.; Mu, Y.; Kwoh, K.C. Fast, accurate, and reliable molecular docking with QuickVina 2. *Bioinformatics*. 2015, 31(13), 2214–2216. DOI: [10.1093/bioinformatics/btv082](https://doi.org/10.1093/bioinformatics/btv082)

- ²⁷Molecular Docking Tutorial: AUTODOCK VINA - PART 1 | Beginners to Advanced. *Sanket Bapet*. YouTube, March 20, 2020, <https://www.youtube.com/watch?v=Sux91FJ3Xe8>, (Accessed 2023-12-11)
- ²⁸Molecular Docking Tutorial: AUTODOCK VINA - PART 2 | Beginners to Advanced. *Sanket Bapet*. YouTube, March 20, 2020, <https://www.youtube.com/watch?v=vU2aNuP3Y8I&t=76s>, (Accessed 2023-12-11)
- ²⁹How to make C60 (buckyballs) in spartan (Wavefunction). *VSU Marine Chemistry*. YouTube, October 30, 2020, https://www.youtube.com/watch?v=lc_W4dbdFYc&t=659s, (Accessed 2023-12-11)